Publications of the Astronomical Society of Australia (PASA), Vol. 31, e027, 23 pages (2014).

doi:10.1017/pasa.2014.26

Absolute Magnitude Calibration for Dwarfs Based on the Colour–Magnitude Diagrams of Galactic Clusters

S. Karaali†,[1,2], E. Yaz Gökçe[1], S. Bilir[1] and S. Tunçel Güçtekin[1]

[1]Department of Astronomy and Space Sciences, Faculty of Science, Istanbul University, 34119, Istanbul, Turkey
[2]Email: karsa@istanbul.edu.tr

(Received December 30, 2013; Accepted May 22, 2014)

Abstract

We present two absolute magnitude calibrations for dwarfs based on colour–magnitude diagrams of Galactic clusters. The combination of the M_g absolute magnitudes of the dwarf fiducial sequences of the clusters M92, M13, M5, NGC 2420, M67, and NGC 6791 with the corresponding metallicities provides absolute magnitude calibration for a given $(g-r)_0$ colour. The calibration is defined in the colour interval $0.25 \leq (g-r)_0 \leq 1.25$ mag and it covers the metallicity interval $-2.15 \leq [Fe/H] \leq +0.37$ dex. The absolute magnitude residuals obtained by the application of the procedure to another set of Galactic clusters lie in the interval $-0.15 \leq \Delta M_g \leq +0.12$ mag. The mean and standard deviation of the residuals are $< \Delta M_g >= -0.002$ and $\sigma = 0.065$ mag, respectively. The calibration of the M_J absolute magnitude in terms of metallicity is carried out by using the fiducial sequences of the clusters M92, M13, 47 Tuc, NGC 2158, and NGC 6791. It is defined in the colour interval $0.90 \leq (V-J)_0 \leq 1.75$ mag and it covers the same metallicity interval of the M_g calibration. The absolute magnitude residuals obtained by the application of the procedure to the cluster M5 ($[Fe/H] = -1.40$ dex) and 46 solar metallicity, $-0.45 \leq [Fe/H] \leq +0.35$ dex, field stars lie in the interval -0.29 and $+0.35$ mag. However, the range of 87% of them is rather shorter, $-0.20 \leq \Delta M_J \leq +0.20$ mag. The mean and standard deviation of all residuals are $< \Delta M_J >= 0.05$ and $\sigma = 0.13$ mag, respectively. The derived relations are applicable to stars older than 4 Gyr for the M_g calibration, and older than 2 Gyr for the M_J calibration. The cited limits are the ages of the youngest calibration clusters in the two systems.

Keywords: globular clusters: individual (M5, M13, M92, 47 Tuc) – (Galaxy:) open clusters: individual (M67, NGC 2158, NGC 2420, NGC 6791) – (stars:) dwarfs – stars: general – stars: late-type – techniques: photometric (Galaxy:)

1 INTRODUCTION

The distance of an astronomical object plays an important role in deriving absolute magnitudes of stars and determining the three-dimensional structure of our Galaxy. For nearby stars, *Hipparcos* (ESA 1997) is the main supplier of the data where a trigonometric parallax has been used. However, for stars at large distances, a photometric parallax is inevitable.

Different methods appeared in the literature related to absolute magnitude determination. Nissen & Schuster (1991) and Laird, Carney, & Latham (1988) used the offset from standard main-sequence for the absolute magnitude determination of dwarfs. The studies of Phleps et al. (2000) and Chen et al. (2001) are based on the colour–absolute magnitude diagrams of some specific clusters whose metal abundances are adopted as representative of a Galactic population, i.e., thin and thick discs, and halo. Siegel et al. (2002) derived two relations, one for solar-like abundances and another for metal-poor stars, between the M_R absolute magnitude and $R-I$ colour index which provide absolute magnitude estimation of dwarfs with different metallicities by means of linear interpolation or extrapolation.

A more recent procedure for absolute magnitude estimation for dwarfs and giants simultaneously is based on the measured atmospheric parameters and the time spent by the star in each region of the H–R diagram. For details of this procedure, we refer to the works of Breddels et al. (2010) and Zwitter et al. (2010).

The most recent absolute magnitude calibrations are those of Karaali, Bilir, & Yaz Gökçe (2012) and Karaali, Bilir & Yaz Gökçe (2013a, 2013b). Karaali et al. combined the colour-apparent magnitude diagrams of Galactic clusters with different metal abundances and their distance moduli, and calibrated the M_V, M_g, M_J, and M_{K_s} absolute magnitudes of red giants in terms of metallicity. Here, we will apply the same procedure to the dwarfs using the Sloan Digital Sky Survey (SDSS; York et al. 2000) and Two Micron All

† Retired.

Table 1. Data for the clusters used in the calibration with SDSS.

Cluster	$E(B-V)$ (mag)	μ_0 (mag)	$[Fe/H]$ (dex)	Ref
M92	0.025	14.72	−2.15	1
M13	0.020	14.38	−1.41	1
M5	0.040	14.37	−1.26	2
NGC 2420	0.040	12.00	−0.37	2
M67	0.038	9.53	−0.04	1
NGC 6791	0.150	13.10	+0.37	3

(1) Gratton et al. (1997), (2) An et al. (2008), (3) Brasseur et al. (2010)

Sky Survey (2MASS; Skrutskie et al. 2006) data, two of the widely used photometric systems in Galactic research. This procedure is different than the ones in Karaali et al. (2003) and Karaali, Bilir, & Tunçel (2005) where the absolute magnitude was calibrated in terms of the parameter $\delta_{0.6}$, the ultraviolet excess relative to the Hyades cluster, reduced to the intrinsic colour $B-V=0.60$ mag. The U ultraviolet magnitude cannot be observed accurately for each star. Whereas, various procedures can be utilized to determine metallicity for a larger set of stars. Hence, for the procedure in this paper, we expect an advantage over the former one.

This paper is the fourth one related to the calibration of absolute magnitudes of stars. The former ones were devoted to red giants, while in this paper the subject is dwarfs. We calibrate the M_g and M_J absolute magnitudes in terms of metallicity. The outline of the paper follows the presentation of the data in Section 2, procedure utilized for calibration in Section 3, and a summary and discussion in Section 4.

2 DATA

We calibrated two different absolute magnitudes, M_g and M_J, in terms of metallicity. Hence, we used two different sets of data. The calibration of g_0 with $(g-r)_0$ is given in Section 2.1, while that for J_0 with $(V-J)_0$ is presented in Section 2.2.

2.1 Data for calibration with SDSS: $g_0 \times (g-r)_0$

Our sample consists of M92, M13, M5, NGC 2420, M67, and NGC 6791 stellar clusters with different metal abundance. The SDSS photometric data of the clusters were taken from An et al. (2008), while the $(g-M_g)_0$ true distance modulus, $E(B-V)$ colour excess, and $[Fe/H]$ iron abundance are from the references in the last column of Table 1. The range of the metallicity is $-2.15 \leq [Fe/H] \leq +0.37$ dex. The g and $g-r$ fiducials of the stellar clusters adapted from An et al. (2008) are given in Table 2. As in our previous works, we used $R_V=3.1$ (Cardelli, Clayton, & Mathis 1989) to obtain the total extinction at the V band. Then, we used the equations of Fan (1999) to calculate the total extinction in A_g and the selective absorption in SDSS, $E(g-r)/A_V=0.341$.

We fitted the $g_0 \times (g-r)_0$ main-sequence of each cluster to a fifth-degree polynomial. The calibration of g_0 is as follows:

$$g_0 = \sum_{i=0}^{5} a_i (g-r)_0^i \tag{1}$$

The numerical values of a_i coefficients are given in Table 3 and the corresponding diagrams are shown in Figure 1. The $(g-r)_0$ values in the second line of the table denote the range of $(g-r)_0$ available for each cluster.

2.2 Data for calibration with 2MASS: $J_0 \times (V-J)_0$

Five clusters with different metallicities, i.e., M92, M13, **NGC 6791**, 47 Tuc, and NGC 2158, were selected for our programme. The J and $V-J$ data for the first three clusters were taken from Brasseur et al. (2010), while those for the clusters of 47 Tuc and NGC 2158 were transformed from the *BVRI* and *gri* data, respectively, as explained in the following. For 47 Tuc, we de-reddened the V, $B-V$, and $R-I$ magnitude and colours of Alcaino et al. (1990) and transformed them to the $(V-J)_0$ colours by the following equation of Bilir et al. (2008):

$$(V-J)_0 = 1.557(B-V)_0 + 0.461(R-I)_0 + 0.049. \tag{2}$$

Then, we combined the V_0 magnitude and $(V-J)_0$ colour and obtained the J_0 magnitude. For the cluster NGC 2158, we obtained the $(V-J)_0$ colours in two steps. First, we transformed the de-reddened g_0, $(g-r)_0$, and $(r-i)_0$ data of Smolinski et al. (2011) to the $(g-J)_0$ colour by using the following equation of Bilir et al. (2008):

$$(g-J)_0 = 1.536(g-r)_0 + 1.400(r-i)_0 + 0.488. \tag{3}$$

Then, the magnitude g_0 is combined with this equation to give the J_0 magnitude, and further, Equation (2) of Chonis & Gaskell (2008) given in the following:

$$V_0 = g_0 - 0.587(g-r)_0 - 0.011, \tag{4}$$

is used in the evaluation of $(V-J)_0$ as follows:

$$(V-J)_0 = (g-J)_0 - 0.587(g-r)_0 - 0.011. \tag{5}$$

The range of the metallicity of the clusters given in iron abundance is $-2.15 \leq [Fe/H] \leq 0.37$ dex. The true distance modulus, μ_0, $E(B-V)$ colour excess, and $[Fe/H]$ iron abundance for the clusters are taken from the authors given in the last column of Table 4. Two references are given for the clusters 47 Tuc and NGC 2158. The metallicity of 47 Tuc is taken from Alcaino et al. (1990), while the colour excess and true distance modulus are from Harris

Table 2. g, r magnitudes, $g-r$, and de-reddened $(g-r)_0$ colours and g_0 magnitudes for the clusters M92, M13, M5, NGC 2420, M67, and NGC 6791 used in the calibration with SDSS.

r	$g-r$	g	$(g-r)_0$	g_0
		M92		
18.750	0.225	18.975	0.199	18.882
19.050	0.240	19.290	0.214	19.197
19.350	0.263	19.613	0.237	19.520
19.650	0.291	19.941	0.265	19.848
19.950	0.326	20.276	0.300	20.183
20.250	0.369	20.619	0.343	20.526
20.550	0.422	20.972	0.396	20.879
20.850	0.483	21.333	0.457	21.240
		M13		
18.750	0.270	19.020	0.249	18.946
19.050	0.288	19.338	0.267	19.264
19.350	0.315	19.665	0.294	19.591
19.650	0.349	19.999	0.328	19.925
19.950	0.391	20.341	0.370	20.267
20.250	0.441	20.691	0.420	20.617
20.550	0.500	21.050	0.479	20.976
20.850	0.569	21.419	0.548	21.345
21.150	0.643	21.793	0.622	21.719
21.450	0.719	22.169	0.698	22.095
21.750	0.798	22.548	0.777	22.474
		M67		
13.500	0.369	13.869	0.329	13.728
13.700	0.388	14.088	0.348	13.947
13.900	0.408	14.308	0.368	14.167
14.100	0.431	14.531	0.391	14.390
14.300	0.465	14.765	0.425	14.624
14.500	0.507	15.007	0.467	14.866
14.700	0.545	15.245	0.505	15.104
14.900	0.579	15.479	0.539	15.338
15.100	0.616	15.716	0.576	15.575
15.300	0.661	15.961	0.621	15.820
15.500	0.713	16.213	0.673	16.072
15.700	0.772	16.472	0.732	16.331
15.900	0.841	16.741	0.801	16.600
16.100	0.912	17.012	0.872	16.871
16.300	0.988	17.288	0.948	17.147
16.500	1.070	17.570	1.030	17.429
16.700	1.147	17.847	1.107	17.706
16.900	1.216	18.116	1.176	17.975
17.100	1.279	18.379	1.239	18.238
17.300	1.330	18.630	1.290	18.489
17.500	1.363	18.863	1.323	18.722
17.700	1.392	19.092	1.352	18.951
17.900	1.419	19.319	1.379	19.178
18.100	1.440	19.540	1.400	19.399
		M5		
18.650	0.290	18.940	0.248	18.791
18.950	0.308	19.258	0.266	19.109
19.250	0.335	19.585	0.293	19.436
19.550	0.368	19.918	0.326	19.769
		M5		
19.850	0.411	20.261	0.369	20.112
20.150	0.463	20.613	0.421	20.464
20.450	0.522	20.972	0.480	20.823
20.750	0.588	21.338	0.546	21.189
21.050	0.665	21.715	0.623	21.566
21.350	0.754	22.104	0.712	21.955
21.650	0.850	22.500	0.808	22.351
		NGC 2420		
15.100	0.235	15.335	0.193	15.186
15.300	0.246	15.546	0.204	15.397
15.500	0.265	15.765	0.223	15.616
15.700	0.290	15.990	0.248	15.841
15.900	0.315	16.215	0.273	16.066
16.100	0.340	16.440	0.298	16.291
16.300	0.367	16.667	0.325	16.518
16.500	0.398	16.898	0.356	16.749
16.700	0.429	17.129	0.387	16.980
16.900	0.463	17.363	0.421	17.214
17.100	0.500	17.600	0.458	17.451
17.300	0.539	17.839	0.497	17.690
17.500	0.586	18.086	0.544	17.937
17.700	0.636	18.336	0.594	18.187
17.900	0.689	18.589	0.647	18.440
18.100	0.748	18.848	0.706	18.699
18.300	0.812	19.112	0.77	18.963
18.500	0.884	19.384	0.842	19.235
18.700	0.958	19.658	0.916	19.509
18.900	1.035	19.935	0.993	19.786
19.100	1.120	20.220	1.078	20.071
19.300	1.195	20.495	1.153	20.346
19.500	1.255	20.755	1.213	20.606
19.700	1.312	21.012	1.270	20.863
19.900	1.360	21.260	1.318	21.111
20.100	1.394	21.494	1.352	21.345
20.300	1.422	21.722	1.380	21.573
20.500	1.438	21.938	1.396	21.789
		NGC 6791		
17.550	0.670	18.220	0.511	17.662
17.750	0.682	18.432	0.523	17.874
18.050	0.715	18.765	0.556	18.207
18.350	0.760	19.110	0.601	18.552
18.650	0.815	19.465	0.656	18.907
18.950	0.886	19.836	0.727	19.278
19.250	0.969	20.219	0.810	19.661
19.550	1.061	20.611	0.902	20.053
19.850	1.162	21.012	1.003	20.454
20.150	1.263	21.413	1.104	20.855
20.450	1.354	21.804	1.195	21.246
20.750	1.431	22.181	1.272	21.623
–	–	–	–	–

Table 3. The values of the coefficients a_i (i =0,. . .,5) in Equation (1).

Cluster	M92	M13	M5	NGC 2420	M67	NGC 6791
$(g-r)_0$ interval	[0.20, 0.46]	[0.25, 0.78]	[0.25, 0.81]	[0.19, 1.40]	[0.33, 1.40]	[0.51, 1.27]
a_5	7289.856	224.151	259.663	8.460	13.044	53.081
a_4	− 12324.726	− 632.530	− 732.851	− 32.353	− 52.757	− 250.015
a_3	8269.137	708.233	813.566	50.359	86.340	468.511
a_2	− 2768.241	− 396.039	− 447.797	− 41.975	− 73.637	− 437.308
a_1	472.894	116.688	128.576	23.339	37.436	207.802
a_0	− 13.697	5.748	4.585	11.978	6.911	− 21.621

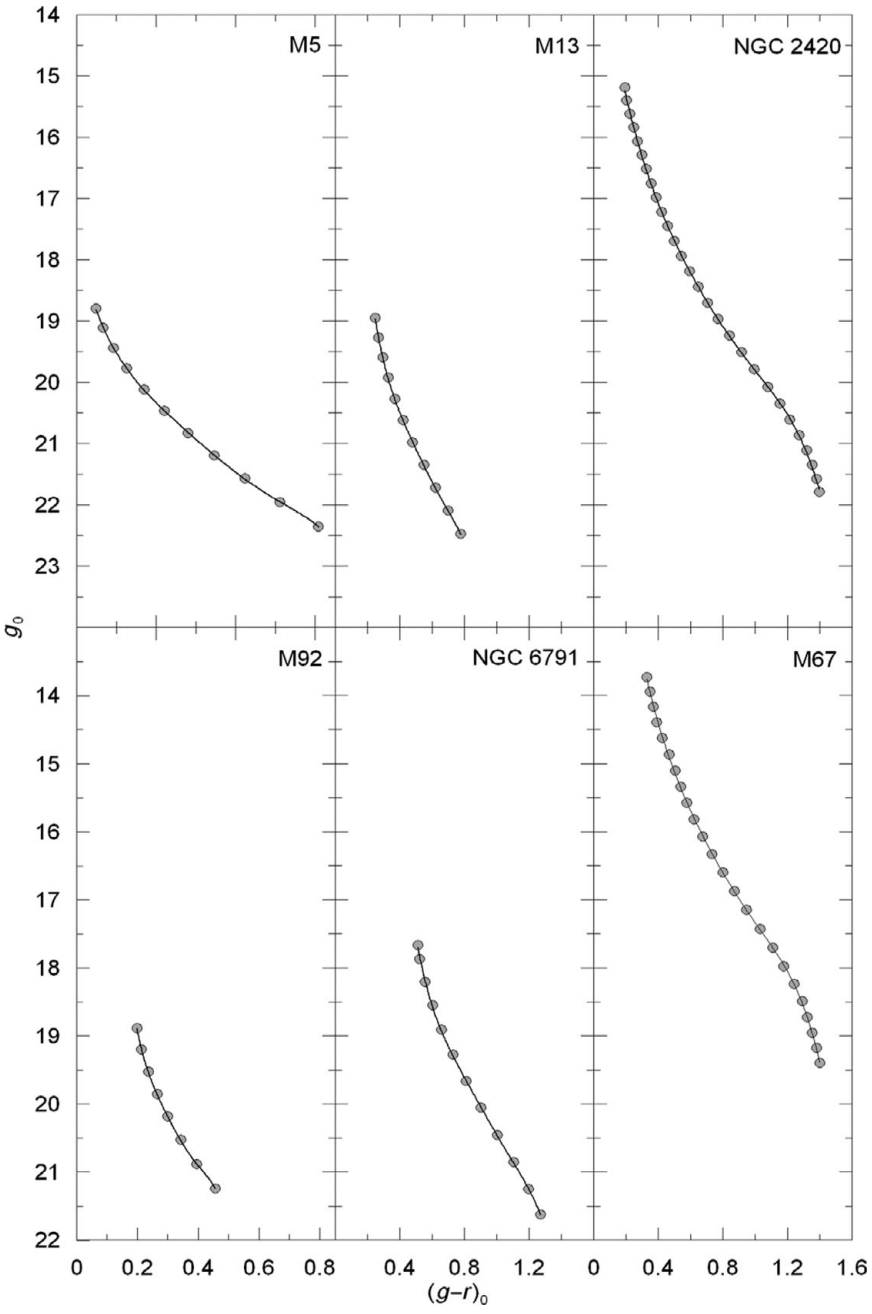

Figure 1. $g_0 \times (g-r)_0$ colour-apparent magnitude diagrams of six stellar clusters used for the absolute magnitude calibration with SDSS.

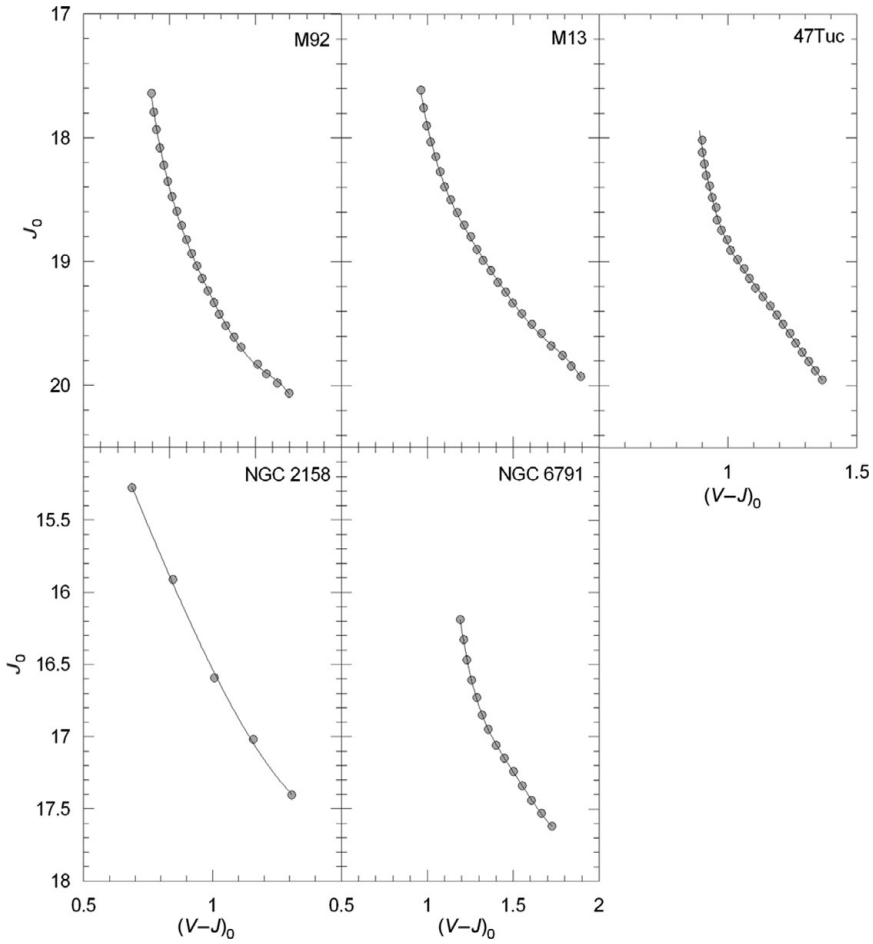

Figure 2. $J_0 \times (V-J)_0$ colour-apparent magnitude diagrams for five clusters used for the M_J absolute magnitude calibration.

Table 4. Data for the clusters used in the calibration with 2MASS.

Cluster	$E(B-V)$ (mag)	μ_0 (mag)	$[Fe/H]$ (dex)	References
M92	0.025	14.72	−2.15	1
M13	0.020	14.38	−1.41	1
47 Tuc	0.220	15.40	−1.27	2, 3
NGC 2158	0.440	13.38	−0.25	4, 5
NGC 6791	0.150	13.10	0.37	6

(1) Gratton et al. (1997), (2) Harris (1996), (3) Alcaino et al. (1990), (4) Smolinski et al. (2011), (5) Arp & Cuffey (1962), (6) Brasseur et al. (2010)

(1996). The metallicity and the colour excess of the cluster NGC 2158 are those of Smolinski et al. (2011), while its distance modulus is reduced from the apparent distance modulus in Arp & Cuffey (1962), i.e., $\mu = 14.74$ mag. Although this distance modulus is old, it provides J_0 and $(V-J)_0$ data which are more agreeable with the colours and magnitudes of the other clusters used in the calibration. The J_0 and $(V-J)_0$ data are presented in Table 5. We adopted the $R = A_V/E(B-V) = 3.1$ to convert the colour excess to the extinction (Cardelli et al. 1989). Then, we used the equations $A_J/E(B-V) = 0.87$ and $E(V-J)/E(B-V) = 2.25$ (McCall 2004) to de-redden the J magnitude and $V-J$ colour, respectively. The de-reddening of the $R-I$ colour used for the cluster 47 Tuc is carried out by the equation $E(R-I)/E(B-V) = 0.60$ (Bilir et al. 2008).

We fitted the $J_0 \times (V-J)_0$ sequence of four clusters to a fifth-degree polynomial, while a third-degree polynomial was sufficient for NGC 2158 due to less data. The calibration of J_0 is as follows:

$$J_0 = \sum_{i=0}^{5} b_i (V-J)_0^i \qquad (6)$$

The numerical values of the coefficients b_i $(i = 0, 1, 2, 3, 4, 5)$ are given in Table 6 and the corresponding diagrams are presented in Figure 2. The $(V-J)_0$ interval in the second line of the table denotes the range of $(V-J)_0$ available for each cluster.

Table 5. Colours and magnitudes for the clusters used in the calibration with 2MASS.

M92					M13					
V	$V-J$	J	$(V-J)_0$	J_0	V	$V-J$	J	$(V-J)_0$	J_0	
21.994	1.883	20.111	1.827	20.089	22.039	2.011	20.028	1.966	20.011	–
21.836	1.752	20.084	1.696	20.062	21.884	1.939	19.945	1.894	19.928	–
21.688	1.684	20.004	1.628	19.982	21.740	1.883	19.857	1.838	19.840	–
21.550	1.621	19.929	1.565	19.907	21.606	1.832	19.774	1.787	19.757	–
21.420	1.570	19.850	1.514	19.828	21.460	1.766	19.694	1.721	19.677	–
21.187	1.474	19.713	1.418	19.691	21.306	1.709	19.597	1.664	19.580	–
21.064	1.433	19.631	1.377	19.609	21.173	1.653	19.520	1.608	19.503	–
20.924	1.384	19.540	1.328	19.518	21.030	1.596	19.434	1.551	19.417	–
20.792	1.347	19.445	1.291	19.423	20.891	1.541	19.350	1.496	19.333	–
20.667	1.314	19.353	1.258	19.331	20.761	1.501	19.260	1.456	19.243	–
20.537	1.280	19.257	1.224	19.235	20.640	1.455	19.185	1.410	19.168	–
20.403	1.247	19.156	1.191	19.134	20.502	1.414	19.088	1.369	19.071	–
20.273	1.216	19.057	1.160	19.035	20.372	1.368	19.004	1.323	18.987	–
20.142	1.186	18.956	1.130	18.934	20.249	1.334	18.915	1.289	18.898	–
20.000	1.155	18.845	1.099	18.823	20.112	1.299	18.813	1.254	18.796	–
19.859	1.127	18.732	1.071	18.710	19.979	1.260	18.719	1.215	18.702	–
19.716	1.099	18.617	1.043	18.595	19.839	1.222	18.619	1.175	18.602	–
19.572	1.073	18.499	1.017	18.477	19.700	1.182	18.518	1.137	18.501	–
19.422	1.047	18.375	0.991	18.353	19.560	1.146	18.414	1.101	18.397	–
19.267	1.023	18.244	0.967	18.222	19.411	1.119	18.292	1.074	18.275	–
19.105	1.000	18.105	0.944	18.083	19.263	1.095	18.168	1.050	18.151	–
18.938	0.980	17.958	0.924	17.936	19.113	1.063	18.050	1.018	18.033	–
18.780	0.965	17.815	0.909	17.793	18.962	1.042	17.920	0.997	17.903	–
18.617	0.953	17.664	0.897	17.642	18.800	1.024	17.776	0.979	17.759	–
					18.637	1.008	17.629	0.963	17.612	–

NGC 6791					NGC 2158					
V	$V-J$	J	$(V-J)_0$	J_0	$(g-r)_0$	g_0	$(r-i)_0$	$(g-J)_0$	$(V-J)_0$	J_0
19.817	2.062	17.755	1.725	17.625	0.123	15.744	−0.018	0.652	0.569	15.092
19.659	2.001	17.658	1.664	17.528	0.208	16.099	0.010	0.821	0.688	15.278
19.515	1.944	17.571	1.607	17.441	0.299	16.947	0.061	1.033	0.846	15.914
19.363	1.889	17.474	1.552	17.344	0.401	17.847	0.107	1.254	1.007	16.593
19.215	1.840	17.375	1.503	17.245	0.498	18.480	0.149	1.462	1.158	17.018
19.067	1.787	17.280	1.450	17.150	0.598	19.075	0.188	1.670	1.308	17.405
18.924	1.738	17.186	1.401	17.056	0.693	19.371	0.217	1.856	**1.438**	**17.515**
18.771	1.692	17.079	1.355	16.949	0.784	19.539	0.244	2.034	**1.563**	**17.505**
18.633	1.656	16.977	1.319	16.847	0.878	19.749	0.293	2.247	**1.720**	**17.502**
18.486	1.625	16.861	1.288	16.731	–	–	–	–	–	–
18.331	1.595	16.736	1.258	16.606	–	–	–	–	–	–
18.172	1.567	16.605	1.230	16.475	–	–	–	–	–	–
18.011	1.548	16.463	1.211	16.333	–	–	–	–	–	–
17.845	1.529	16.316	1.192	16.186	–	–	–	–	–	–

47 Tuc										
V	$B-V$	$R-I$	V_0	$(B-V)_0$	$(R-I)_0$	$(V-J)_0$	J_0			
19.700	0.662	0.487	19.018	0.442	0.355	0.901	18.117	–	–	–
19.800	0.666	0.489	19.118	0.446	0.357	0.908	18.210	–	–	–
19.900	0.669	0.493	19.218	0.449	0.361	0.915	18.303	–	–	–
20.000	0.676	0.500	19.318	0.456	0.368	0.929	18.389	–	–	–
20.100	0.681	0.506	19.418	0.461	0.374	0.939	18.479	–	–	–
20.300	0.691	0.514	19.618	0.471	0.382	0.958	18.660	–	–	–
20.400	0.700	0.518	19.718	0.480	0.386	0.974	18.744	–	–	–
20.500	0.714	0.520	19.818	0.494	0.388	0.997	18.821	–	–	–
20.600	0.722	0.522	19.918	0.502	0.390	1.010	18.908	–	–	–
20.700	0.737	0.528	20.018	0.517	0.396	1.037	18.981	–	–	–
20.800	0.752	0.534	20.118	0.532	0.402	1.063	19.055	–	–	–
20.900	0.764	0.539	20.218	0.544	0.407	1.084	19.134	–	–	–
21.000	0.777	0.545	20.318	0.557	0.413	1.107	19.211	–	–	–
21.100	0.794	0.550	20.418	0.574	0.418	1.135	19.283	–	–	–
21.200	0.809	0.561	20.518	0.589	0.429	1.164	19.354	–	–	–
21.300	0.824	0.567	20.618	0.604	0.435	1.190	19.428	–	–	–
21.400	0.838	0.571	20.718	0.618	0.439	1.214	19.504	–	–	–
21.500	0.856	0.569	20.818	0.636	0.437	1.241	19.577	–	–	–

Table 5. Continued.

47 Tuc V	$B-V$	$R-I$	V_0	$(B-V)_0$	$(R-I)_0$	$(V-J)_0$	J_0			
21.600	0.870	0.568	20.918	0.650	0.436	1.262	19.656	–	–	–
21.700	0.887	0.569	21.018	0.667	0.437	1.289	19.729	–	–	–
21.800	0.902	0.573	21.118	0.682	0.441	1.314	19.804	–	–	–
21.900	0.917	0.577	21.218	0.697	0.445	1.339	19.879	–	–	–
22.000	0.932	0.584	21.318	0.712	0.452	1.366	19.952	–	–	–

Table 6. Numerical values of the coefficients b_i ($i = 0, 1, 2, 3, 4, 5$).

Cluster $(V-J)_0$ interval	M92 [0.90, 1.83]	M13 [0.96, 1.96]	47 Tuc [0.90, 1.37]	NGC 2158 [0.57, 1.31]	NGC 6791 [1.19, 1.72]
b_5	13.498	11.536	152.580	—	74.861
b_4	− 97.365	− 88.498	− 957.780	—	− 583.990
b_3	278.950	269.890	2395.100	− 1.791	1819.900
b_2	− 399.070	− 409.920	− 2982.400	3.395	− 2832.700
b_1	288.640	312.580	1852.200	2.183	2204.800
b_0	− 66.255	− 77.700	− 440.800	12.745	− 670.490

Table 7. M_g absolute magnitudes estimated for a set of $(g-r)_0$ colours for six clusters used in the calibration with SDSS.

$(g-r)_0$	M92 M_g	M13 M_g	M5 M_g	NGC 2420 M_g	M67 M_g	NGC 6791 M_g
0.20	4.199	–	–	3.321	–	–
0.25	4.972	4.603	4.475	3.858	–	–
0.30	5.460	5.275	5.148	4.320	–	–
0.35	5.864	5.746	5.611	4.723	4.442	–
0.40	6.178	6.107	5.965	5.079	4.883	–
0.45	6.462	6.417	6.273	5.399	5.261	–
0.50	–	6.704	6.563	5.691	5.593	–
0.55	–	6.978	6.840	5.961	5.890	5.024
0.60	–	7.240	7.100	6.213	6.160	5.451
0.65	–	7.485	7.333	6.450	6.410	5.779
0.70	–	7.717	7.537	6.675	6.644	6.048
0.75	–	7.953	7.728	6.887	6.865	6.283
0.80	–	–	7.945	7.089	7.073	6.503
0.85	–	–	–	7.281	7.271	6.717
0.90	–	–	–	7.464	7.458	6.927
0.95	–	–	–	7.639	7.636	7.136
1.00	–	–	–	7.808	7.807	7.340
1.05	–	–	–	7.976	7.975	7.539
1.10	–	–	–	8.146	8.145	7.734
1.15	–	–	–	8.327	8.324	7.930
1.20	–	–	–	8.526	8.523	8.139
1.25	–	–	–	8.755	8.757	8.381
1.30	–	–	–	9.028	9.043	–
1.35	–	–	–	9.363	9.402	–

3 THE PROCEDURE

3.1 Absolute magnitude as a function of metallicity

We adopted the procedure used in our previous papers (Karaali et al. 2013a, 2013b) which consists of calibration of an absolute magnitude as a function of metallicity. We calibrated the M_g and M_J absolute magnitudes in terms of metallicity for a given $(g-r)_0$ and $(V-J)_0$ colour, respectively.

3.1.1 Calibration of M_g in terms of metallicity

We estimated the M_g absolute magnitude for the $(g-r)_0$ colours given in Table 7 for the cluster sample in Table 1 by combining the g_0 apparent magnitude evaluated by

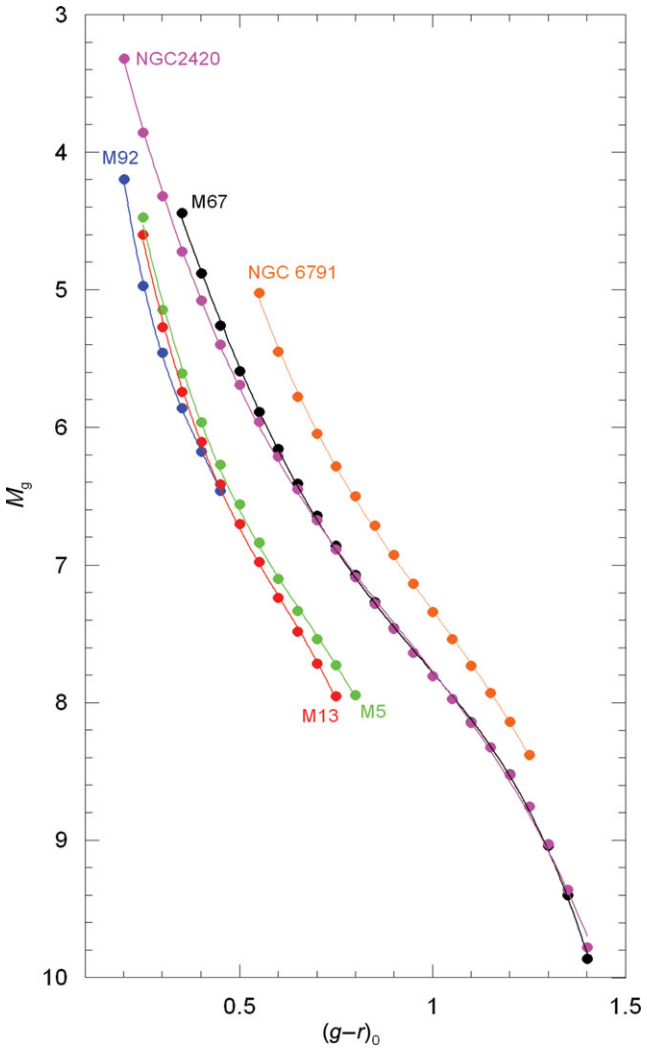

Figure 3. $M_g \times (g-r)_0$ colour-magnitude diagram for six clusters used for the absolute magnitude calibration with SDSS.

Table 8. M_g absolute magnitudes and $[Fe/H]$ metallicities for six $(g-r)_0$ intervals.

$(g-r)_0$ (mag)	$[Fe/H]$ (dex)	M_g (mag)	$(g-r)_0$ (mag)	$[Fe/H]$ (dex)	M_g (mag)
0.25	−2.15	4.972	0.80	−1.26	7.945
	−1.41	4.603		−0.37	7.089
	−1.26	4.475		−0.04	7.073
	−0.37	3.858		0.37	6.503
0.40	−2.15	6.178	0.95	−0.37	7.639
	−1.41	6.107		−0.04	7.636
	−1.26	5.965		0.37	7.136
	−0.37	5.079	1.20	−0.37	8.526
	−0.04	4.883		−0.04	8.523
0.65	−1.41	7.485		0.37	8.139
	−1.26	7.333	–	–	–
	−0.37	6.450	–	–	–
	−0.04	6.410	–	–	–
	0.37	5.779	–	–	–

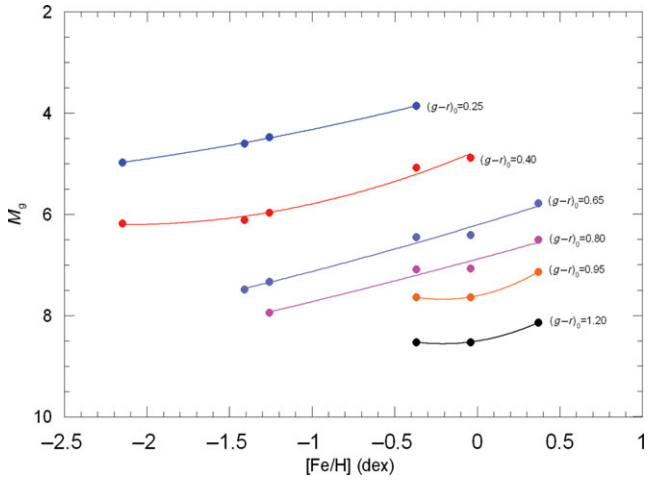

Figure 4. Calibration of the absolute magnitude M_g as a function of metallicity $[Fe/H]$ for six colour indices.

Equation (1) and the true distance modulus (μ_0) of the cluster in question, i.e.,

$$M_g = g_0 - \mu_0. \tag{7}$$

The $M_g \times (g-r)_0$ absolute magnitude–colour diagrams are plotted in Figure 3. The absolute magnitudes of the clusters M13 ($[Fe/H] = -1.41$ dex) and M5 ($[Fe/H] = -1.26$ dex) are close to each other for a given colour. Similar case is valid for the clusters NGC 2420 ($[Fe/H] = -0.37$ dex) and M67 ($[Fe/H] = -0.04$ dex). However, we used both couples to obtain a better absolute magnitude calibration.

In this phase, M_g absolute magnitudes can be fitted to the corresponding $[Fe/H]$ metal abundance for a given $(g-r)_0$ colour index and obtain the required calibration. This procedure is executed for the colour indices $(g-r)_0 = 0.25$, 0.40, 0.65, 0.80, 0.95, and 1.20 (Table 8 and Figure 4). The absolute magnitudes in all colour indices are fitted to a second-degree polynomial with (squared) correlation coefficients between $R^2 = 0.962$ and $R^2 = 0.999$, where the first one corresponds to the absolute magnitudes for the colour index $(g-r)_0 = 0.80$ mag (but see the following paragraph). A third-degree polynomial (Figure 5) increases the correlation coefficient to $R^2 = 1$. However, it causes a flat distribution in the metallicity interval $-0.90 \leq [Fe/H] \leq -0.40$ dex, resulting almost a constant absolute magnitude in this metallicity interval which contradicts the trends of absolute magnitudes for small colour indices, such as $(g-r)_0 = 0.35$ mag, where the correlation coefficient is high, $R^2 = 0.991$. We shall see in Section 3.2 that the application of the third-degree polynomial in question causes larger residuals than the ones for a quadratic polynomial, $\Delta M = -0.360$ and 0.067 mag, respectively.

The number of clusters in the absolute magnitude calibration for the colour indices $0.82 \leq (g-r)_0 \leq 1.25$ mag is only three, i.e., NGC 2420, M67, and NGC 6791 with metallicities $[Fe/H] = -0.37$, $[Fe/H] = -0.04$, and $[Fe/H] =$

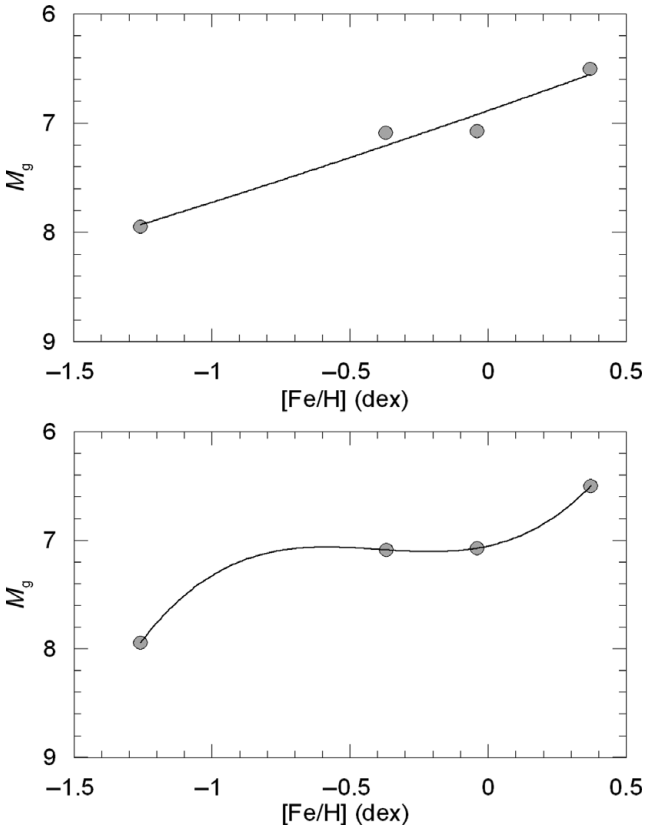

Figure 5. Comparison the trends of the absolute magnitude calibrations with polynomial degrees $n = 2$ (upper panel) and $n = 3$ (lower panel) for the colour index $(g - r)_0 = 0.80$ mag.

0.37 dex, respectively. Additionally, the absolute magnitudes of the clusters NGC 2420 and M67 are close to each other. If we fit a quadratic polynomial to three metallicity and absolute magnitude couples, the segment corresponding to the interval $-0.37 \leq [Fe/H] \leq -0.04$ dex will perform a concave shape resulting in (estimated) absolute magnitudes larger than the ones for the cluster NGC 2420 which is opposite to the sense of the argument used in our work, i.e., the absolute magnitude of a dwarf with a given metallicity and colour should be brighter than one relatively more metal-poor. Hence, we fitted a linear equation to three metallicity and absolute magnitude couples in question (Figure 6b).

The procedure can be applied to any $(g - r)_0$ colour interval for which the sample clusters are defined. The $(g - r)_0$ domains of the clusters are different. Hence, we adopted this interval in our study as $0.25 \leq (g - r)_0 \leq 1.25$ mag where at least three clusters are defined, and we evaluated M_g absolute magnitudes for each colour. Then, we combined them with the corresponding $[Fe/H]$ metallicities and obtained the final calibrations. The general form of the equation for the calibrations is as follows:

$$M_g = c_0 + c_1 X + c_2 X^2, \tag{8}$$

where $X = [Fe/H]$. The absolute magnitudes estimated via Equation (7) for 101 $(g - r)_0$ colour indices and the corresponding c_i $(i = 0, 1, 2)$ coefficients are given in Table 9. The coefficients c_1 and c_0 for the linear equation

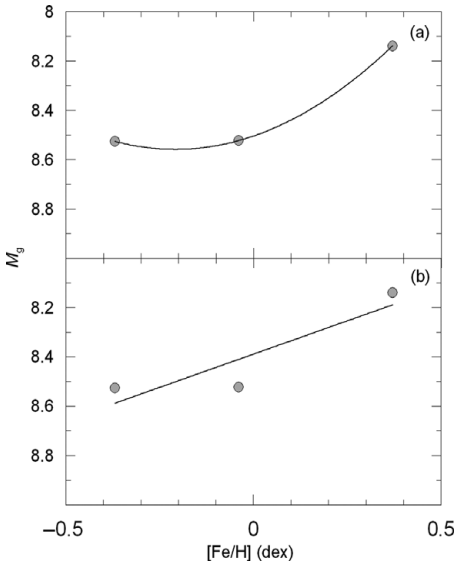

Figure 6. Two fittings to the metallicities and absolute magnitudes for the colour index $(g - r)_0 = 1.20$ dex. (a) a quadratic polynomial to three couples and (b) a linear polynomial to three couples.

$$M_g = c_0 + c_1 X, \tag{9}$$

which are valid for the colour interval $0.82 \leq (g - r)_0 \leq 1.25$ are also tabulated in Table 9. The diagrams for the calibrations are not given in the paper because of space constraints. One can use any dataset taken from Table 9 depending on the desire for accuracy, and apply it to stars whose iron abundances are available.

3.1.2 Calibration of M_J in terms of metallicity

We estimated the M_J absolute magnitude for the $(V - J)_0$ colours given in Table 10 for the cluster sample in Table 4 by combining the J_0 apparent magnitude evaluated by Equation (6) and the true distance modulus (μ_0) of the cluster in question, i.e.,

$$M_J = J_0 - \mu_0. \tag{10}$$

The absolute magnitudes versus $(V - J)_0$ colours are plotted in Figure 7. We fitted the M_J absolute magnitudes to the corresponding $[Fe/H]$ metallicity for the following $(V - J)_0$ colour indices and obtained the required calibrations just for the exhibition of the procedure: $(V - J)_0 = 1.00$, 1.15, 1.30, 1.50, and 1.70. The results are given in Table 11 and Figure 8. The absolute magnitudes in all colour indices are fitted to a quadratic polynomial with (squared) correlation coefficients (R^2) between 0.9667 and 1, where the first one corresponds to the absolute magnitudes for the colour index $(V - J)_0 = 1.15$ mag.

PASA, 31, e027 (2014)
doi:10.1017/pasa.2014.26

Table 9. Absolute magnitudes estimated for six Galactic clusters and the numerical values of c_i ($i = 0, 1, 2$) coefficients in Equations (8) and (9).

	M92	M13	M5	NGC 2420	M67	NGC 6791							M92	M13	M5	NGC 2420	M67	NGC 6791	(cont.)				
$(g-r)_0$	M_g	M_g	M_g	M_g	M_g	M_g	c_2	c_1	c_0	R^2	$[Fe/H]$ interval	$(g-r)_0$	M_g	M_g	M_g	M_g	M_g	M_g	c_2	c_1	c_0	R^2	$[Fe/H]$ interval
0.25	4.972	4.603	4.475	3.858	–	–	−0.0977	−0.8738	3.5469	0.9990	[−2.15, −0.37]	0.76	–	8.004	7.767	6.929	6.908	6.328	0.0094	−0.8681	6.7093	0.9754	[−1.41, 0.37]
0.26	5.081	4.759	4.633	3.956	–	–	−0.1663	−1.0527	3.5880	0.9991	[−2.15, −0.37]	0.77	–	8.057	7.808	6.970	6.950	6.372	0.0182	−0.8609	6.7507	0.9749	[−1.41, 0.37]
0.27	5.182	4.904	4.778	4.051	–	–	−0.2255	−1.2054	3.6346	0.9991	[−2.15, −0.37]	0.78	–	8.113	7.851	7.010	6.991	6.416	0.0285	−0.8538	6.7915	0.9744	[−1.41, 0.37]
0.28	5.278	5.037	4.912	4.143	–	–	−0.2754	−1.3335	3.6863	0.9991	[−2.15, −0.37]	0.79	–	–	7.896	7.050	7.033	6.460	−0.0492	−0.8850	6.8449	0.9625	[−1.26, 0.37]
0.29	5.371	5.161	5.035	4.233	–	–	−0.3166	−1.4388	3.7426	0.9991	[−2.15, −0.37]	0.80	–	–	7.945	7.089	7.073	6.503	−0.0403	−0.8803	6.8854	0.9625	[−1.26, 0.37]
0.30	5.460	5.275	5.148	4.320	–	–	−0.3498	−1.5235	3.8030	0.9990	[−2.15, −0.37]	0.81	–	–	7.998	7.129	7.114	6.546	−0.0284	−0.8755	6.9252	0.9628	[−1.26, 0.37]
0.31	5.546	5.382	5.254	4.405	–	–	−0.3758	−1.5901	3.8667	0.9989	[−2.15, −0.37]	0.82	–	–	–	7.167	7.154	6.589	–	−0.8054	6.9593	0.8181	[−0.37, 0.37]
0.32	5.630	5.482	5.352	4.488	–	–	−0.3958	−1.6412	3.9330	0.9989	[−2.15, −0.37]	0.83	–	–	–	7.206	7.193	6.632	–	−0.7995	6.9995	0.8169	[−0.37, 0.37]
0.33	5.711	5.575	5.443	4.568	–	–	−0.4108	−1.6794	4.0013	0.9988	[−2.15, −0.37]	0.84	–	–	–	7.244	7.232	6.674	–	−0.7932	7.0395	0.8157	[−0.37, 0.37]
0.34	5.789	5.663	5.530	4.646	–	–	−0.4220	−1.7075	4.0707	0.9987	[−2.15, −0.37]	0.85	–	–	–	7.281	7.271	6.717	–	−0.7866	7.0791	0.8145	[−0.37, 0.37]
0.35	5.864	5.746	5.611	4.723	4.442	–	−0.3313	−1.4360	4.3272	0.9913	[−2.15, −0.04]	0.86	–	–	–	7.319	7.309	6.759	–	−0.7796	7.1185	0.8134	[−0.37, 0.37]
0.36	5.934	5.824	5.688	4.797	4.536	–	−0.3281	−1.4217	4.4159	0.9893	[−2.15, −0.04]	0.87	–	–	–	7.355	7.347	6.801	–	−0.7722	7.1575	0.8124	[−0.37, 0.37]
0.37	6.001	5.900	5.761	4.870	4.627	–	−0.325	−1.4070	4.5020	0.9873	[−2.15, −0.04]	0.88	–	–	–	7.392	7.384	6.843	–	−0.7644	7.1963	0.8113	[−0.37, 0.37]
0.38	6.064	5.971	5.832	4.941	4.715	–	−0.3226	−1.3927	4.5857	0.9852	[−2.15, −0.04]	0.89	–	–	–	7.428	7.421	6.885	–	−0.7562	7.2349	0.8104	[−0.37, 0.37]
0.39	6.123	6.040	5.900	5.011	4.800	–	−0.3211	−1.3796	4.6670	0.9829	[−2.15, −0.04]	0.90	–	–	–	7.464	7.458	6.927	–	−0.7477	7.2732	0.8094	[−0.37, 0.37]
0.40	6.178	6.107	5.965	5.079	4.883	–	−0.3203	−1.3677	4.7459	0.9806	[−2.15, −0.04]	0.91	–	–	–	7.499	7.494	6.969	–	−0.7389	7.3112	0.8085	[−0.37, 0.37]
0.41	6.231	6.172	6.029	5.146	4.963	–	−0.3201	−1.3570	4.8225	0.9782	[−2.15, −0.04]	0.92	–	–	–	7.535	7.530	7.011	–	−0.7298	7.3490	0.8077	[−0.37, 0.37]
0.42	6.283	6.235	6.092	5.211	5.040	–	−0.3198	−1.3465	4.8972	0.9758	[−2.15, −0.04]	0.93	–	–	–	7.570	7.566	7.053	–	−0.7205	7.3865	0.8069	[−0.37, 0.37]
0.43	6.337	6.297	6.153	5.275	5.116	–	−0.3183	−1.3349	4.9702	0.9736	[−2.15, −0.04]	0.94	–	–	–	7.604	7.601	7.094	–	−0.7110	7.4238	0.8062	[−0.37, 0.37]
0.44	6.396	6.357	6.214	5.337	5.190	–	−0.3142	−1.3201	5.0417	0.9717	[−2.15, −0.04]	0.95	–	–	–	7.639	7.636	7.136	–	−0.7014	7.4609	0.8055	[−0.37, 0.37]
0.45	6.462	6.417	6.273	5.399	5.261	–	−0.3054	−1.2994	5.1124	0.9706	[−2.15, −0.04]	0.96	–	–	–	7.673	7.671	7.177	–	−0.6916	7.4977	0.8049	[−0.37, 0.37]
0.46	6.541	6.475	6.332	5.459	5.331	–	−0.2895	−1.2693	5.1827	0.9704	[−2.15, −0.04]	0.97	–	–	–	7.707	7.705	7.218	–	−0.6818	7.5343	0.8044	[−0.37, 0.37]
0.47	–	6.533	6.390	5.519	5.399	–	0.3926	−0.2839	5.3772	0.9980	[−1.41, −0.04]	0.98	–	–	–	7.741	7.739	7.259	–	−0.6721	7.5708	0.8039	[−0.37, 0.37]
0.48	–	6.591	6.448	5.577	5.465	–	0.4071	−0.2573	5.4441	0.9978	[−1.41, −0.04]	0.99	–	–	–	7.775	7.773	7.300	–	−0.6624	7.6070	0.8035	[−0.37, 0.37]
0.49	–	6.647	6.506	5.634	5.530	–	0.4207	−0.2329	5.5093	0.9976	[−1.41, −0.04]	1.00	–	–	–	7.808	7.807	7.340	–	−0.6529	7.6431	0.8032	[−0.37, 0.37]

PASA, 31, e027 (2014)
doi:10.1017/pasa.2014.26

Table 9. Continued.

	M92	M13	M5	NGC 2420	M67	NGC 6791							M92	M13	M5	NGC 2420	M67	NGC 6791	(cont.)				
$(g-r)_0$	M_g	M_g	M_g	M_g	M_g	M_g	c_2	c_1	c_0	R^2	$[Fe/H]$ interval	$(g-r)_0$	M_g	M_g	M_g	M_g	M_g	M_g	c_2	c_1	c_0	R^2	$[Fe/H]$ interval
0.50	–	6.704	6.563	5.691	5.593	–	0.4332	−0.2106	5.5730	0.9974	[−1.41, −0.04]	1.01	–	–	–	7.842	7.841	7.380	–	−0.6435	7.6791	0.8030	[−0.37, 0.37]
0.51	–	6.760	6.619	5.747	5.655	–	0.4450	−0.1902	5.6353	0.9972	[−1.41, −0.04]	1.02	–	–	–	7.875	7.875	7.420	–	−0.6344	7.7149	0.8029	[−0.37, 0.37]
0.52	–	6.815	6.675	5.801	5.715	–	0.4560	−0.1715	5.6961	0.9970	[−1.41, −0.04]	1.03	–	–	–	7.909	7.908	7.460	–	−0.6255	7.7506	0.8028	[−0.37, 0.37]
0.53	–	6.870	6.731	5.855	5.775	–	0.4664	−0.1542	5.7557	0.9968	[−1.41, −0.04]	1.04	–	–	–	7.942	7.942	7.500	–	−0.6170	7.7862	0.8029	[−0.37, 0.37]
0.54	–	6.924	6.786	5.908	5.833	–	0.4763	−0.1382	5.8141	0.9966	[−1.41, −0.04]	1.05	–	–	–	7.976	7.975	7.539	–	−0.6089	7.8218	0.8030	[−0.37, 0.37]
0.55	–	6.978	6.840	5.961	5.890	5.024	−0.3039	−1.3558	5.6378	0.9745	[−1.41, 0.37]	1.06	–	–	–	8.009	8.009	7.578	–	−0.6011	7.8574	0.8031	[−0.37, 0.37]
0.56	–	7.032	6.894	6.013	5.946	5.120	−0.2652	−1.2953	5.7028	0.9753	[−1.41, 0.37]	1.07	–	–	–	8.043	8.042	7.617	–	−0.5938	7.8930	0.8034	[−0.37, 0.37]
0.57	–	7.085	6.947	6.064	6.001	5.209	−0.2306	−1.2414	5.7658	0.9760	[−1.41, 0.37]	1.08	–	–	–	8.077	8.076	7.656	–	−0.5870	7.9287	0.8037	[−0.37, 0.37]
0.58	–	7.137	6.999	6.114	6.055	5.294	−0.1999	−1.1936	5.8267	0.9767	[−1.41, 0.37]	1.09	–	–	–	8.112	8.110	7.695	–	−0.5807	7.9645	0.8041	[−0.37, 0.37]
0.59	–	7.189	7.050	6.164	6.108	5.375	−0.1727	−1.1513	5.8859	0.9772	[−1.41, 0.37]	1.10	–	–	–	8.146	8.145	7.734	–	−0.5748	8.0006	0.8045	[−0.37, 0.37]
0.60	–	7.240	7.100	6.213	6.160	5.451	−0.1487	−1.1140	5.9433	0.9776	[−1.41, 0.37]	1.11	–	–	–	8.181	8.179	7.773	–	−0.5695	8.0369	0.8049	[−0.37, 0.37]
0.61	–	7.290	7.149	6.261	6.212	5.523	−0.1276	−1.0811	5.9992	0.9780	[−1.41, 0.37]	1.12	–	–	–	8.217	8.215	7.812	–	−0.5646	8.0735	0.8054	[−0.37, 0.37]
0.62	–	7.340	7.197	6.309	6.262	5.591	−0.1092	−1.0523	6.0537	0.9783	[−1.41, 0.37]	1.13	–	–	–	8.253	8.250	7.851	–	−0.5602	8.1105	0.8058	[−0.37, 0.37]
0.63	–	7.389	7.243	6.357	6.312	5.657	−0.0932	−1.0270	6.1068	0.9785	[−1.41, 0.37]	1.14	–	–	–	8.289	8.287	7.890	–	−0.5563	8.1480	0.8061	[−0.37, 0.37]
0.64	–	7.437	7.289	6.404	6.362	5.719	−0.0794	−1.0048	6.1586	0.9786	[−1.41, 0.37]	1.15	–	–	–	8.327	8.324	7.930	–	−0.5528	8.1861	0.8064	[−0.37, 0.37]
0.65	–	7.485	7.333	6.450	6.410	5.779	−0.0674	−0.9854	6.2093	0.9786	[−1.41, 0.37]	1.16	–	–	–	8.365	8.362	7.970	–	−0.5496	8.2249	0.8066	[−0.37, 0.37]
0.66	–	7.532	7.376	6.496	6.458	5.836	−0.0571	−0.9684	6.2589	0.9786	[−1.41, 0.37]	1.17	–	–	–	8.403	8.401	8.011	–	−0.5468	8.2644	0.8067	[−0.37, 0.37]
0.67	–	7.579	7.418	6.541	6.506	5.892	−0.0482	−0.9533	6.3075	0.9786	[−1.41, 0.37]	1.18	–	–	–	8.443	8.440	8.053	–	−0.5441	8.3048	0.8066	[−0.37, 0.37]
0.68	–	7.625	7.459	6.586	6.552	5.945	−0.0405	−0.9401	6.3552	0.9784	[−1.41, 0.37]	1.19	–	–	–	8.484	8.481	8.095	–	−0.5416	8.3463	0.8063	[−0.37, 0.37]
0.69	–	7.671	7.498	6.631	6.599	5.997	−0.0336	−0.9283	6.4020	0.9782	[−1.41, 0.37]	1.20	–	–	–	8.526	8.523	8.139	–	−0.5391	8.3888	0.8058	[−0.37, 0.37]
0.70	–	7.717	7.537	6.675	6.644	6.048	−0.0275	−0.9176	6.4480	0.9780	[−1.41, 0.37]	1.21	–	–	–	8.569	8.567	8.184	–	−0.5365	8.4327	0.8050	[−0.37, 0.37]
0.71	–	7.763	7.576	6.718	6.689	6.097	−0.0218	−0.9080	6.4932	0.9777	[−1.41, 0.37]	1.22	–	–	–	8.613	8.612	8.230	–	−0.5337	8.4780	0.8038	[−0.37, 0.37]
0.72	–	7.809	7.613	6.761	6.734	6.145	−0.0163	−0.8991	6.5378	0.9773	[−1.41, 0.37]	1.23	–	–	–	8.659	8.659	8.278	–	−0.5305	8.5248	0.8023	[−0.37, 0.37]
0.73	–	7.856	7.651	6.804	6.778	6.192	−0.0107	−0.8908	6.5816	0.9769	[−1.41, 0.37]	1.24	–	–	–	8.706	8.707	8.328	–	−0.5267	8.5734	0.8003	[−0.37, 0.37]
0.74	–	7.904	7.689	6.846	6.822	6.238	−0.0047	−0.8830	6.6248	0.9764	[−1.41, 0.37]	1.25	–	–	–	8.755	8.757	8.381	–	−0.5221	8.6240	0.7977	[−0.37, 0.37]
0.75	–	7.953	7.728	6.887	6.865	6.283	−0.0019	−0.8755	6.6674	0.9759	[−1.41, 0.37]	–	–	–	–	–	–	–	–	–	–	–	–

Table 10. M_J absolute magnitudes estimated for a set of $(V-J)_0$ colours for five clusters used for the calibration with 2MASS. The absolute magnitudes with boldface are not considered in the calibration (see text).

Cluster $(V-J)_0$ (mag)	M92 M_J (mag)	M13 M_J (mag)	47 Tuc M_J (mag)	NGC 2158 M_J (mag)	NGC 6791 M_J (mag)
0.90	3.00	—	2.76	2.77	—
0.95	3.38	3.16	3.22	2.97	—
1.00	3.68	3.51	3.50	3.15	—
1.05	3.92	3.78	3.69	3.33	—
1.10	4.12	3.99	3.84	3.49	—
1.15	4.30	4.16	3.98	3.64	—
1.20	4.45	4.30	4.13	3.78	3.19
1.25	4.59	4.42	4.29	**3.90**	3.51
1.30	4.71	4.53	4.44	**4.00**	3.73
1.35	4.83	4.64	4.59	**4.09**	3.88
1.40	4.94	4.74	—	**4.16**	4.01
1.45	5.04	4.83	—	—	4.12
1.50	5.12	4.93	—	—	4.22
1.55	5.20	5.02	—	—	4.33
1.60	5.25	5.11	—	—	4.43
1.65	5.30	5.18	—	—	4.52
1.70	5.33	5.26	—	—	4.61
1.75	5.36	5.32	—	—	4.71
1.80	**5.38**	**5.39**	—	—	—
1.85	—	**5.45**	—	—	—
1.90	—	**5.51**	—	—	—
1.95	—	**5.60**	—	—	—

We adopted the interval in $0.90 < (V-J)_0 \leq 1.75$ mag, where at least three clusters are defined, for the application of the procedure and we evaluated M_J absolute magnitudes for each colour. Then, we combined them with the corresponding $[Fe/H]$ metallicities and obtained the final calibrations. The general form of the equation for the calibrations is as follows:

$$M_J = d_0 + d_1 X + d_2 X^2, \tag{11}$$

where $X = [Fe/H]$. The absolute magnitudes estimated via Equation (10) for 85 $(V-J)_o$ colour indices and the corresponding d_i $(i = 0,\ 1,\ 2)$ coefficients are given in Table 12.

3.2 Application of the procedure

We have two absolute magnitude calibrations, M_g and M_J, in terms of metallicity. Hence, we can apply each of them to a set of data.

3.2.1 Application of the $M_g \times [Fe/H]$ calibration

The procedure is applied to four clusters with different metal abundances (M53, M3, M71, and M35). The reason of preferring stellar clusters instead of individual field dwarfs is that clusters provide absolute magnitudes for comparison with the ones estimated by the method. The choice of test clusters as well as the calibrator ones is arbitrary. Hence, we

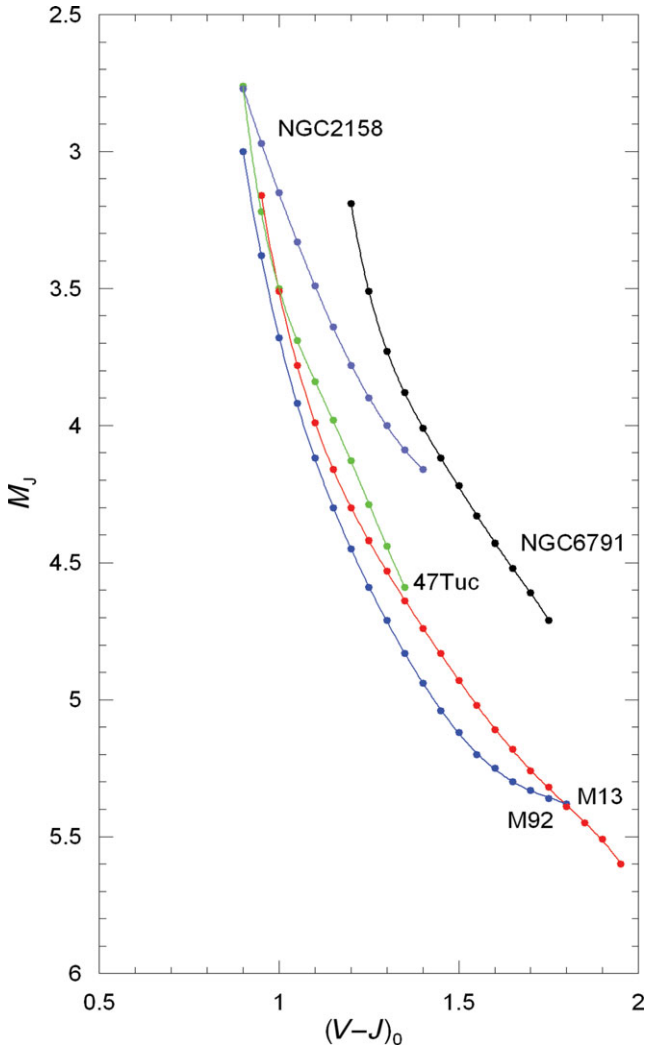

Figure 7. $M_J \times (V-J)_0$ colour-absolute magnitude diagrams for five clusters used for the absolute magnitude calibration with 2MASS.

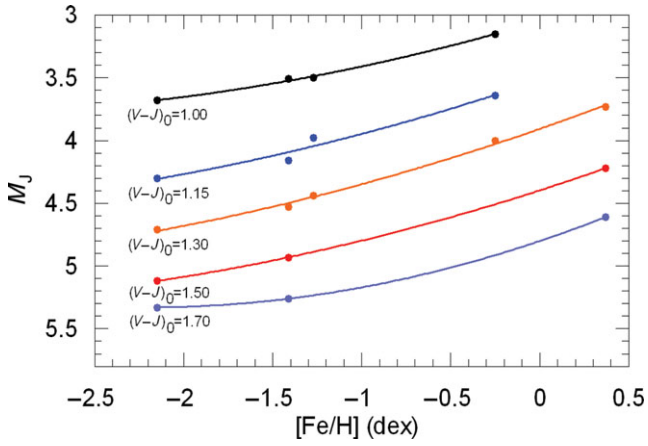

Figure 8. Calibration of the absolute magnitude M_J as a function of metallicity $[Fe/H]$ for five colour indices.

Table 11. M_J absolute magnitudes and $[Fe/H]$ metallicities for five $(V-J)_0$ intervals.

$(V-J)_0$ (mag)	$[Fe/H]$ (dex)	M_J (mag)
1.00	−2.15	3.68
	−1.41	3.51
	−1.27	3.50
	−0.25	3.15
1.15	−2.15	4.30
	−1.41	4.16
	−1.27	3.98
	−0.25	3.64
1.30	−2.15	4.71
	−1.41	4.53
	−1.27	4.44
	−0.25	4.00
	0.37	3.73
1.50	−2.15	5.12
	−1.41	4.93
	0.37	4.22
1.70	−2.15	5.33
	−1.41	5.26
	0.37	4.61

did not involve these clusters into the calibration set but we used them to confirm the robustness of the procedure. In the case of field stars, one needs their distances or trigonometric parallaxes in addition to their g_0 and $(g-r)_0$ data in order to evaluate their absolute magnitudes for their comparison with the ones estimated by the procedure in our work. However, such stars are rare in the literature. The parameters of stellar clusters and $(g,\ g-r)$ photometric data are given in Tables 13 and 14, respectively. The colour-apparent magnitude diagrams of the Galactic clusters used for the application of the procedure are shown in Figure 9. The g and the $g-r$ data of the clusters M53, M3, and M71 are taken from An et al. (2008), whereas those of M35 are transformed from the V and $B-V$ data in von Hippel et al. (2002) by the reduced transformation equations of Chonis & Gaskell (2008) given in the following:

$$g = V + 0.642 \times (B-V) - 0.135,$$
$$g - r = 1.094 \times (B-V) - 0.248. \quad (12)$$

The reason of this choice is to obtain the g and $g-r$ data for a relatively metal rich cluster with a large colour range. The metallicity of M35 is $[Fe/H] = -0.16$ dex, and it covers the colour range of $-0.30 \leq (g-r)_0 \leq 1.40$ mag. However, the application could be carried out for the colour interval $0.35 \leq (g-r)_0 \leq 1.25$ mag, due to the restriction of our calibrations for the metallicity $[Fe/H] = -0.16$ dex (see Table 9).

We evaluated the M_g absolute magnitude by Equation (8) for a set of $(g-r)_0$ colour indices where the clusters are defined. The results are given in Table 15. The columns refer to (1) $(g-r)_0$, colour index; (2) $(M_g)_{ev}$, the absolute magnitude estimated by the procedure; (3) $(M_g)_{cl}$, absolute magnitude for a cluster estimated by its colour-magnitude diagram; and (4) ΔM, absolute magnitude residuals. Also, the metallicity for each cluster is indicated near the name of the cluster. The differences between the absolute magnitudes estimated by the procedure presented in this study and those evaluated via colour–magnitude diagrams of the clusters (the residuals) lie between −0.15 and +0.12 mag. The mean and the standard deviation of the residuals are $< \Delta M_g >= -0.002$ and $\sigma = 0.065$ mag, respectively. The distribution of the residuals is given in Table 16 and Figure 10.

The linear (Equation (9)) is valid for the colours $(g-r)_0 \geq 0.82$. Hence, we could apply it to only cluster M35. We used the c_1 and c_0 coefficients in Table 9 and evaluated the $(M_g)_{ev}$ absolute magnitudes for nine $(g-r)_0$ colours, i.e. 0.85, 0.90, 0.95, 1.0, 1.05, 1.10, 1.15, 1.20, and 1.25 mag. Then, we compared them with the corresponding ones, $(M_g)_{cl}$. The mean of the residuals and the standard deviation for this set of data are $< \Delta M >= -0.102$ and $\sigma = 0.094$ mag, respectively.

3.2.2 Application of the $M_J \times [Fe/H]$ calibration

We applied the procedure to the cluster M5 and to a set of field stars with solar metallicity as explained in the following. The reason of choosing a cluster is that it provides absolute magnitudes for comparison with the ones estimated by the procedure. The colour excess, $E(B-V) = 0.03$ mag and the metallicity $[Fe/H] = -1.40$ dex of the cluster are taken from Reid (1997), while for the apparent distance modulus we adopted the one of Brasseur et al. (2010), $\mu = 14.45$ mag. Sarajedini et al. (2004) published the 2MASS magnitudes, V magnitudes, metallicities, and parallaxes of 54 field stars. Parallaxes provide absolute magnitudes for comparison with the ones estimated by our procedure, and this is the reason of choosing this sample of stars. The range of the metallicity is $-0.45 \leq [Fe/H] \leq +0.35$ dex, i.e., the stars are of solar metallicity. Hence, their combination with (relatively) metal-poor stars in cluster M5 provides a good sample for the application of the procedure. Two stars, Hip 69301 and Hip 84164, are omitted due to their large relative parallax errors, $\sigma_\pi/\pi = 0.16$ and 0.09, respectively. Also, six stars which fall off the colour domain of our procedure, i.e. $(V-J)_0 > 1.75$ mag, could not be included into our programme. The $V-J$ colours and J magnitudes of M5 cluster were de-reddened by the equations given in Section 3.1.2, while all the magnitudes in Sarajedini et al. (2004) were assumed as unaffected from the interstellar extinction due to the proximity of the field stars to the Sun, $d < 75$ pc. The results are given in Table 17 and Figure 11. The data of the field stars in columns (1)–(6) are original, while those in (7)–(9) are evaluated in this paper. The distance (d) was evaluated by using the corresponding parallax, and the absolute magnitude M_J was calculated by the well known Pogson formula.

Table 12. M_J absolute magnitudes estimated for five Galactic clusters and the numerical values of d_i ($i = 0, 1, 2$) coefficients in Equation (11).

Cluster $(V-J)_0$	M92 M_J	M13 M_J	47 Tuc M_J	NGC 2158 M_J	NGC 6791 M_J	d_2	d_1	d_0	R^2	$[Fe/H]$ interval (dex)
0.91	3.08	—	2.87	2.81	—	0.0946	0.0856	2.8282	1.000	[−2.15, −0.25]
0.92	3.16	—	2.97	2.85	—	0.0507	−0.0411	2.8382	1.000	[−2.15, −0.25]
0.93	3.24	—	3.06	2.89	—	0.0150	−0.1461	2.8529	1.000	[−2.15, −0.25]
0.94	3.31	—	3.14	2.93	—	−0.0133	−0.2318	2.8715	1.000	[−2.15, −0.25]
0.95	3.38	3.16	3.22	2.97	—	0.0122	−0.1831	2.9226	0.953	[−2.15, −0.25]
0.96	3.44	3.24	3.29	3.00	—	−0.0086	−0.2482	2.9450	0.967	[−2.15, −0.25]
0.97	3.51	3.31	3.35	3.04	—	−0.0256	−0.3029	2.9694	0.978	[−2.15, −0.25]
0.98	3.57	3.38	3.40	3.08	—	−0.0394	−0.3485	2.9954	0.987	[−2.15, −0.25]
0.99	3.62	3.45	3.45	3.12	—	−0.0502	−0.3860	3.0229	0.993	[−2.15, −0.25]
1.00	3.68	3.51	3.50	3.15	—	−0.0585	−0.4164	3.0516	0.997	[−2.15, −0.25]
1.01	3.73	3.57	3.54	3.19	—	−0.0646	−0.4405	3.0813	0.999	[−2.15, −0.25]
1.02	3.78	3.62	3.58	3.22	—	−0.0688	−0.4593	3.1119	1.000	[−2.15, −0.25]
1.03	3.83	3.68	3.62	3.26	—	−0.0714	−0.4734	3.1431	0.999	[−2.15, −0.25]
1.04	3.88	3.73	3.66	3.29	—	−0.0728	−0.4836	3.1747	0.997	[−2.15, −0.25]
1.05	3.92	3.78	3.69	3.33	—	−0.0731	−0.4906	3.2067	0.994	[−2.15, −0.25]
1.06	3.96	3.82	3.72	3.36	—	−0.0725	−0.4949	3.2389	0.991	[−2.15, −0.25]
1.07	4.01	3.87	3.75	3.39	—	−0.0714	−0.4970	3.2711	0.987	[−2.15, −0.25]
1.08	4.05	3.91	3.78	3.43	—	−0.0697	−0.4975	3.3033	0.983	[−2.15, −0.25]
1.09	4.09	3.95	3.81	3.46	—	−0.0678	−0.4968	3.3353	0.980	[−2.15, −0.25]
1.10	4.12	3.99	3.84	3.49	—	−0.0657	−0.4953	3.3670	0.976	[−2.15, −0.25]
1.11	4.16	4.02	3.87	3.52	—	−0.0635	−0.4933	3.3984	0.973	[−2.15, −0.25]
1.12	4.20	4.06	3.90	3.55	—	−0.0614	−0.4911	3.4294	0.971	[−2.15, −0.25]
1.13	4.23	4.09	3.93	3.58	—	−0.0595	−0.4889	3.4599	0.969	[−2.15, −0.25]
1.14	4.26	4.13	3.95	3.61	—	−0.0578	−0.4871	3.4898	0.967	[−2.15, −0.25]
1.15	4.30	4.16	3.98	3.64	—	−0.0564	−0.4857	3.5192	0.967	[−2.15, −0.25]
1.16	4.33	4.19	4.01	3.67	—	−0.0554	−0.4850	3.5478	0.967	[−2.15, −0.25]
1.17	4.36	4.22	4.04	3.70	—	−0.0547	−0.4850	3.5758	0.967	[−2.15, −0.25]
1.18	4.39	4.24	4.07	3.72	—	−0.0544	−0.4859	3.6030	0.969	[−2.15, −0.25]
1.19	4.42	4.27	4.10	3.75	—	−0.0546	−0.4878	3.6295	0.970	[−2.15, −0.25]
1.20	4.45	4.30	4.13	3.78	3.19	−0.1490	−0.7434	3.5189	0.983	[−2.15, 0.37]
1.21	4.48	4.32	4.16	3.80	3.26	−0.1324	−0.6998	3.5693	0.986	[−2.15, 0.37]
1.22	4.51	4.35	4.19	3.83	3.33	−0.1179	−0.6617	3.6165	0.989	[−2.15, 0.37]
1.23	4.53	4.37	4.22	3.85	3.40	−0.1052	−0.6284	3.6609	0.991	[−2.15, 0.37]
1.24	4.56	4.40	4.26	3.88	3.45	−0.0942	−0.5996	3.7025	0.993	[−2.15, 0.37]
1.25	4.59	4.42	4.29	3.90	3.51	−0.0847	−0.5748	3.7416	0.995	[−2.15, 0.37]
1.26	4.61	4.44	4.32	3.92	3.56	−0.0765	−0.5536	3.7785	0.996	[−2.15, 0.37]
1.27	4.64	4.46	4.35	3.94	3.61	−0.0696	−0.5356	3.8133	0.997	[−2.15, 0.37]
1.28	4.67	4.49	4.38	3.96	3.65	−0.0636	−0.5205	3.8462	0.997	[−2.15, 0.37]
1.29	4.69	4.51	4.41	3.98	3.69	−0.0586	−0.5079	3.8773	0.998	[−2.15, 0.37]
1.30	4.71	4.53	4.44	4.00	3.73	−0.0544	−0.4975	3.9069	0.997	[−2.15, 0.37]
1.31	4.74	4.55	4.47	4.02	3.76	−0.0509	−0.4890	3.9349	0.997	[−2.15, 0.37]
1.32	4.76	4.57	4.50	—	3.80	−0.0614	−0.4941	3.9860	0.999	[−2.15, 0.37]
1.33	4.79	4.59	4.53	—	3.83	−0.0614	−0.4908	4.0159	1.000	[−2.15, 0.37]
1.34	4.81	4.61	4.56	—	3.86	−0.0618	−0.4888	4.0447	1.000	[−2.15, 0.37]
1.35	4.83	4.64	4.59	—	3.88	−0.0625	−0.4877	4.0725	1.000	[−2.15, 0.37]
1.36	4.85	4.66	—	—	3.91	−0.0635	−0.4876	4.0995	1.000	[−2.15, 0.37]
1.37	4.88	4.68	—	—	3.94	−0.0647	−0.4882	4.1256	1.000	[−2.15, 0.37]
1.38	4.90	4.70	—	—	3.96	−0.0556	−0.4712	4.1426	1.000	[−2.15, 0.37]
1.39	4.92	4.72	—	—	3.98	−0.0541	−0.4674	4.1650	1.000	[−2.15, 0.37]
1.40	4.94	4.74	—	—	4.01	−0.0528	−0.4642	4.1870	1.000	[−2.15, 0.37]
1.41	4.96	4.76	—	—	4.03	−0.0518	−0.4614	4.2087	1.000	[−2.15, 0.37]
1.42	4.98	4.78	—	—	4.05	−0.0511	−0.4591	4.2301	1.000	[−2.15, 0.37]
1.43	5.00	4.80	—	—	4.08	−0.0506	−0.4572	4.2514	1.000	[−2.15, 0.37]
1.44	5.02	4.81	—	—	4.10	−0.0503	−0.4556	4.2725	1.000	[−2.15, 0.37]
1.45	5.04	4.83	—	—	4.12	−0.0502	−0.4543	4.2935	1.000	[−2.15, 0.37]
1.46	5.06	4.85	—	—	4.14	−0.0503	−0.4533	4.3145	1.000	[−2.15, 0.37]
1.47	5.07	4.87	—	—	4.16	−0.0507	−0.4525	4.3354	1.000	[−2.15, 0.37]
1.48	5.09	4.89	—	—	4.18	−0.0512	−0.4519	4.3563	1.000	[−2.15, 0.37]
1.49	5.11	4.91	—	—	4.20	−0.0519	−0.4514	4.3771	1.000	[−2.15, 0.37]
1.50	5.12	4.93	—	—	4.22	−0.0528	−0.4511	4.3980	1.000	[−2.15, 0.37]

Table 12. Continued.

Cluster $(V-J)_0$	M92 M_J	M13 M_J	47 Tuc M_J	NGC 2158 M_J	NGC 6791 M_J	d_2	d_1	d_0	R^2	$[Fe/H]$ interval (dex)
1.51	5.14	4.95	—	—	4.24	−0.0539	−0.4510	4.4188	1.000	[−2.15, 0.37]
1.52	5.15	4.97	—	—	4.27	−0.0551	−0.4510	4.4397	1.000	[−2.15, 0.37]
1.53	5.17	4.98	—	—	4.29	−0.0566	−0.4512	4.4605	1.000	[−2.15, 0.37]
1.54	5.18	5.00	—	—	4.31	−0.0582	−0.4515	4.4813	1.000	[−2.15, 0.37]
1.55	5.20	5.02	—	—	4.33	−0.0600	−0.4519	4.5020	1.000	[−2.15, 0.37]
1.56	5.21	5.04	—	—	4.35	−0.0620	−0.4525	4.5227	1.000	[−2.15, 0.37]
1.57	5.22	5.05	—	—	4.37	−0.0641	−0.4532	4.5433	1.000	[−2.15, 0.37]
1.58	5.23	5.07	—	—	4.39	−0.0665	−0.4541	4.5638	1.000	[−2.15, 0.37]
1.59	5.24	5.09	—	—	4.41	−0.0689	−0.4550	4.5843	1.000	[−2.15, 0.37]
1.60	5.25	5.11	—	—	4.43	−0.0715	−0.4561	4.6046	1.000	[−2.15, 0.37]
1.61	5.26	5.12	—	—	4.45	−0.0743	−0.4573	4.6248	1.000	[−2.15, 0.37]
1.62	5.27	5.14	—	—	4.46	−0.0772	−0.4587	4.6448	1.000	[−2.15, 0.37]
1.63	5.28	5.15	—	—	4.48	−0.0803	−0.4601	4.6647	1.000	[−2.15, 0.37]
1.64	5.29	5.17	—	—	4.50	−0.0834	−0.4616	4.6845	1.000	[−2.15, 0.37]
1.65	5.30	5.18	—	—	4.52	−0.0867	−0.4631	4.7041	1.000	[−2.15, 0.37]
1.66	5.31	5.20	—	—	4.54	−0.0900	−0.4647	4.7235	1.000	[−2.15, 0.37]
1.67	5.31	5.21	—	—	4.56	−0.0934	−0.4663	4.7429	1.000	[−2.15, 0.37]
1.68	5.32	5.23	—	—	4.58	−0.0968	−0.4678	4.7621	1.000	[−2.15, 0.37]
1.69	5.33	5.24	—	—	4.59	−0.1003	−0.4692	4.7812	1.000	[−2.15, 0.37]
1.70	5.33	5.26	—	—	4.61	−0.1038	−0.4705	4.8002	1.000	[−2.15, 0.37]
1.71	5.34	5.27	—	—	4.63	−0.1072	−0.4715	4.8193	1.000	[−2.15, 0.37]
1.72	5.34	5.28	—	—	4.65	−0.1105	−0.4723	4.8384	1.000	[−2.15, 0.37]
1.73	5.35	5.30	—	—	4.67	−0.1137	−0.4726	4.8575	1.000	[−2.15, 0.37]
1.74	5.35	5.31	—	—	4.69	−0.1168	−0.4725	4.8768	1.000	[−2.15, 0.37]
1.75	5.36	5.32	—	—	4.71	−0.1197	−0.4718	4.8963	1.000	[−2.15, 0.37]

Table 13. Data for the clusters used for the application of the procedure with SDSS.

Cluster	$E(B-V)$ (mag)	μ_0 (mag)	$[Fe/H]$ (dex)	Ref
M53	0.021	16.21	−2.06	1,2
M3	0.01	14.83	−1.46	3,4,5
M71	0.32	13.02	−0.73	3
M35	0.19	9.62	−0.16	6

(1) Smolinski et al. (2011), (2) Ferro et al. (2011), (3) An et al. (2008), (4) Saad & Lee (2001), (5) Di Criscienzo, Marconi, & Caputo (2004), (6) Sarajedini, Mathieu, & Platais (2003)

We evaluated the M_J absolute magnitude by Equation (11) for two sets of $(V-J)_0$ colour indices. The first set covers the domain of the cluster M5 (Table 18a), while the second one consists of $(V-J)_0$ colour indices of the field stars (Table 18b). The columns in Table 18a refer to (1) $(V-J)_0$ colour index, (2) $(M_J)_{cl}$, the absolute magnitude estimated by the combination of the colour–magnitude diagram and the true distance modulus of the cluster M5, (3) $(M_J)_{ev}$, the absolute magnitude estimated by the procedure, and (4) ΔM, absolute magnitude residuals. For metallicity, we adopted the one of cluster M5, i.e. $[Fe/H] = -1.40$ dex. The columns in Table 18b refer to (1) $(V-J)_0$ colour index of the field star, (2) $(M_J)_{\pi}$, the absolute magnitude estimated by the parallax of the field star, (3) $[Fe/H]$, the metallicity of the field star, (4) $(M_J)_{ev}$, the absolute magnitude estimated by the procedure, and (5) ΔM, absolute magnitude residuals. The total residuals lie between −0.29 and +0.39 mag. The extreme residuals $\Delta M = -1.03$ and +0.56 mag which are marked in boldface in Table 18b correspond to stars Hip 84164 and Hip 69301 whose relative parallax errors are high, as mentioned above. Hence, they are not considered in the calculations of the mean residual and standard deviation. However, the range of 87% of them is rather shorter, i.e. $-0.20 < \Delta M \leq +0.20$ mag. The mean and the standard deviation of all residuals, except the two extreme ones, are $< \Delta M_J >= 0.05$ and $\sigma = 0.13$ mag. The distribution of the residuals is also given in Table 19 and Figure 12. We state that the cluster fiducials provide more accurate absolute magnitudes than the ones for the field stars. Actually, the mean and the standard deviation of the residuals for the fiducials are $< \Delta M_J >= 0.04$ and $\sigma = 0.05$ mag, whereas those for the field stars are $< \Delta M_J >= 0.06$, $\sigma = 0.16$ mag, respectively.

4 SUMMARY AND DISCUSSION

We presented two absolute magnitude calibrations for dwarfs based on the colour magnitude diagrams of Galactic clusters with different metallicities. For the calibration of M_g, we used the clusters M92, M13, M5, NGC 2420, M67, and NGC 6791. We combined the calibrations between g_0 and $(g-r)_0$ for each cluster with their true distance modulus and evaluated a set of absolute magnitudes for the $(g-r)_0$ range of each cluster. Then, we fitted the M_g absolute magnitudes in terms

Table 14. Fiducial dwarf sequence for the galactic clusters used in the application of the procedure with SDSS.

$g-r$	g	$(g-r)_0$	g_0	$B-V$	V	$(B-V)_0$	V_0	$(g-r)_0$	g_0
M53				M35					
0.263	21.113	0.241	21.035	0.70	14.42	0.51	13.83	0.31	14.02
0.291	21.441	0.269	21.363	0.80	15.06	0.61	14.47	0.42	14.73
0.324	21.774	0.302	21.696	0.90	15.61	0.71	15.02	0.53	15.34
0.362	22.112	0.340	22.034	1.00	16.00	0.81	15.41	0.64	15.80
M71				1.10	16.52	0.91	15.93	0.75	16.38
0.658	19.008	0.320	17.819	1.19	16.85	1.00	16.26	0.85	16.77
0.683	19.333	0.345	18.144	1.31	17.30	1.12	16.71	0.98	17.30
0.716	19.666	0.378	18.477	1.35	17.50	1.16	16.91	1.02	17.52
0.757	20.007	0.419	18.818	1.55	18.40	1.36	17.81	1.24	18.55
M3				1.71	19.10	1.52	18.51	1.41	19.35
0.357	20.507	0.3464	20.470	–	–	–	–	–	–
0.400	20.850	0.3894	20.813	–	–	–	–	–	–
0.451	21.201	0.4404	21.164	–	–	–	–	–	–
0.509	21.559	0.4984	21.522	–	–	–	–	–	–
0.574	21.924	0.5634	21.887	–	–	–	–	–	–
0.640	22.290	0.6294	22.253	–	–	–	–	–	–

Table 15. Absolute magnitudes ($(M_g)_{ev}$) and residuals (ΔM) estimated by the procedure explained in our work. $(M_g)_{cl}$ denotes the absolute magnitude evaluated by means of colour - magnitude diagram of the cluster.

1 $(g-r)_0$	2 $(M_g)_{ev}$	3 $(M_g)_{cl}$	4 ΔM	1 $(g-r)_0$	2 $(M_g)_{ev}$	3 $(M_g)_{cl}$	4 ΔM	1 $(g-r)_0$	2 $(M_g)_{ev}$	3 $(M_g)_{cl}$	4 ΔM
M53 ($[Fe/H]=-2.06$ dex)				M3 ($[Fe/H]=-1.46$ dex)				M71 ($[Fe/H]=-0.73$ dex)			
0.25	4.932	4.936	−0.004	0.35	5.718	5.671	0.047	0.32	4.920	4.806	0.114
0.26	5.051	5.051	−0.001	0.36	5.792	5.753	0.039	0.33	5.008	4.936	0.072
0.27	5.161	5.163	−0.002	0.37	5.863	5.833	0.031	0.34	5.092	5.059	0.033
0.28	5.265	5.270	−0.005	0.38	5.931	5.910	0.021	0.35	5.199	5.176	0.023
0.29	5.363	5.373	−0.010	0.39	5.997	5.986	0.011	0.36	5.279	5.286	−0.007
0.30	5.457	5.471	−0.014	0.40	6.060	6.059	0.001	0.37	5.356	5.389	−0.033
0.31	5.548	5.566	−0.018	0.41	6.121	6.130	−0.009	0.38	5.430	5.485	−0.055
0.32	5.634	5.656	−0.022	0.42	6.181	6.199	−0.018	0.39	5.503	5.575	−0.072
0.33	5.718	5.743	−0.025	0.43	6.241	6.267	−0.026	0.40	5.574	5.658	−0.085
0.34	5.797	5.825	−0.027	0.44	6.299	6.333	−0.034	0.41	5.643	5.735	−0.092
–	–	–	–	0.45	6.359	6.397	−0.039	–	–	–	–
–	–	–	–	0.46	6.419	6.460	−0.042	–	–	–	–
M35 ($[Fe/H]=-0.16$ dex)				M35 (cont.)				M35 (cont.)			
0.35	4.55	4.68	−0.127	0.70	6.59	6.51	0.082	1.00	7.82	7.81	0.009
0.40	4.96	4.98	−0.019	0.75	6.81	6.74	0.069	1.05	7.99	8.03	−0.038
0.45	5.31	5.26	0.053	0.80	7.03	6.96	0.067	1.10	8.16	8.24	−0.085
0.50	5.62	5.53	0.086	0.85	7.29	7.17	0.117	1.15	8.34	8.46	−0.126
0.55	5.85	5.79	0.056	0.90	7.48	7.39	0.089	1.20	8.54	8.69	−0.154
0.60	6.12	6.04	0.077	0.95	7.65	7.60	0.053	1.25	8.77	8.92	−0.155
0.65	6.37	6.28	0.085	–	–	–	–	–	–	–	–

of the iron metallicity, $[Fe/H]$, by a quadratic polynomial for a given $(g-r)_0$ colour index. Our absolute magnitude calibrations cover the range $0.25 \leq (g-r)_0 \leq 1.25$ mag.

We applied the procedure to another set of Galactic cluster, i.e. M53, M3, M71, and M35 and compared the absolute magnitudes estimated by this procedure with those evaluated via a combination of the fiducial g_0, $(g-r)_0$ sequence and the true distance modulus for each cluster. The residuals lie between −0.15 and +0.12 mag, and their mean and standard deviations are $<\Delta M>=-0.002$ and $\sigma=0.065$ mag. The range of the residuals estimated for the red giants with SDSS was $-0.28 \leq \Delta M \leq +0.43$ mag (Karaali et al. 2013a), larger than the one for the dwarfs estimated in this study. Also, their mean and standard deviation were larger, i.e. $<\Delta M>=0.169$ and $\sigma=0.140$. The difference between two sets of residuals originates mainly from the different trends of the colour–magnitude diagrams of red giants and dwarfs, i.e., the colour–magnitude diagram of red

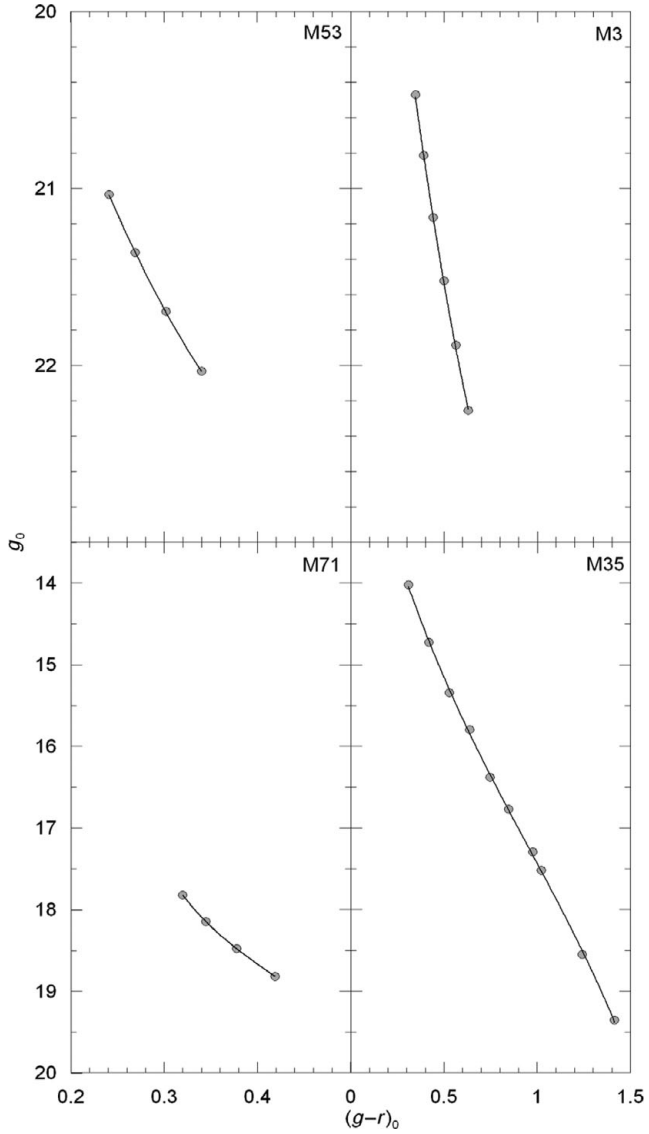

Figure 9. $g_0 \times (g-r)_0$ colour-apparent magnitude diagrams for the Galactic clusters used for the application of the procedure.

Table 16. Distribution of the residuals. N denotes the number of stars.

ΔM_g-interval	$< \Delta M_g >$	N
$[-0.15, -0.10]$	-0.140	4
$[-0.10, -0.05]$	-0.078	5
$[-0.05, 0.00]$	-0.020	20
$[0.00, 0.05]$	0.024	9
$[0.05, 0.10]$	0.072	11
$[0.10, 0.15]$	0.115	2

giants for a given cluster is steeper than the one for dwarfs of the same cluster, and any error in $(g-r)_0$ results in larger colour errors within the steeper diagram.

The range of the $(B-V)_0$ colour in Karaali et al. (2003) who estimated absolute magnitudes for dwarfs by absolute magnitude offsets is $0.3 \leq (B-V)_0 \leq 1.1$ mag which corresponds to $0.1 \leq (g-r)_0 \leq 0.9$ mag, shorter than the one cited in our study, i.e. $0.25 \leq (g-r)_0 \leq 1.25$ mag. That is, there is an improvement on our procedure with respect to the one of Karaali et al. (2003).

For the calibration of M_J, we used the clusters M92, M13, 47 Tuc, NGC 2158 and NGC 6791. We combined the calibrations between J_0 and $(V-J)_0$ for each cluster with their true distance modulus and evaluated a set of absolute magnitudes for the $(V-J)_0$ range of each cluster. Then, we calibrated the M_J absolute magnitudes in terms of the iron metallicity, $[Fe/H]$, by a quadratic polynomial for all cluster. Our absolute magnitude calibrations cover the range $0.90 < (V-J)_0 \leq 1.75$ mag.

This is our fourth paper devoted to the calibration of the absolute magnitudes based on the colour–magnitude diagrams of Galactic clusters, and it is the first time that we

Table 17. Data for the cluster M5 and the field stars used for the application of the procedure with 2MASS.

M5				
V (mag)	$V-J$ (mag)	J (mag)	$(V-J)_0$ (mag)	J_0 (mag)
21.95	2.01	19.94	1.940	19.914
21.84	1.96	19.88	1.890	19.854
21.60	1.84	19.76	1.770	19.734
21.37	1.74	19.63	1.670	19.604
21.16	1.65	19.51	1.580	19.484
20.95	1.56	19.39	1.490	19.364
20.75	1.50	19.25	1.430	19.224
20.55	1.43	19.12	1.360	19.094
20.36	1.36	19.00	1.290	18.974
20.16	1.30	18.86	1.230	18.834
19.96	1.26	18.70	1.190	18.674
19.75	1.21	18.54	1.140	18.514
19.53	1.17	18.36	1.100	18.334
19.31	1.12	18.19	1.050	18.164
19.07	1.08	17.99	1.010	17.964
18.83	1.05	17.78	0.980	17.754
18.59	1.03	17.56	0.960	17.534

Field stars

(1) HIP	(2) V (mag)	(3) π (mas)	(4) σ_π (mas)	(5) $[Fe/H]$ (dex)	(6) J (mag)	(7) $V-J$ (mag)	(8) d (pc)	(9) M_J (mag)
39088	9.239	19.52	0.83	0.334	7.806	1.433	51.2	4.258
39342	7.166	57.88	0.58	−0.043	5.647	1.519	17.3	4.460
40051	8.778	29.86	0.82	0.090	7.131	1.647	33.5	4.506
40419	8.272	29.39	1.14	−0.483	6.895	1.377	34.0	4.236
42074	7.330	45.95	1.01	0.044	5.917	1.413	21.8	4.228
42281	8.688	27.02	1.18	0.310	7.168	1.520	37.0	4.326
42914	8.183	32.14	0.82	−0.095	6.832	1.351	31.1	4.367
44341	8.028	32.18	1.09	0.210	6.628	1.400	31.1	4.166
44719	8.410	25.83	0.91	0.034	7.014	1.396	38.7	4.075
46580	7.203	78.87	1.02	−0.110	5.429	1.774	12.7	4.914
46422	8.855	25.40	0.83	−0.204	7.348	1.507	39.4	4.372
48754	8.524	27.18	1.10	−0.321	7.158	1.366	36.8	4.329
50032	9.068	23.19	1.09	0.022	7.538	1.530	43.1	4.365
50274	8.966	22.42	0.82	−0.246	7.561	1.405	44.6	4.314
50713	9.360	17.30	1.26	0.134	7.971	1.389	57.8	4.161
50782	7.769	37.30	1.31	0.063	6.399	1.370	26.8	4.258
51297	8.859	29.83	1.03	−0.318	7.379	1.480	33.5	4.752
54538	9.738	16.39	1.24	−0.156	8.286	1.452	61.0	4.359
55210	7.275	45.48	1.00	−0.222	5.914	1.361	21.9	4.203
57321	9.370	18.94	1.33	−0.073	7.989	1.381	52.8	4.376
58536	8.411	27.81	1.05	0.033	7.034	1.377	36.0	4.255
58949	8.166	30.58	1.02	0.008	6.775	1.391	32.7	4.202
59572	7.918	32.30	1.02	0.374	6.571	1.347	31.0	4.117
59639	8.633	31.54	0.83	0.027	7.036	1.597	31.7	4.530
61291	7.143	61.83	0.63	−0.205	5.626	1.517	16.2	4.582
61998	8.441	27.45	1.13	−0.242	7.143	1.298	36.4	4.336
62942	8.247	38.12	1.44	−0.094	6.661	1.586	26.2	4.567
64103	9.668	14.41	1.48	−0.290	8.431	1.237	69.4	4.224
64125	9.402	19.08	1.28	−0.288	7.882	1.520	52.4	4.285
65121	8.594	32.83	1.08	0.142	6.929	1.665	30.5	4.510
65646	10.773	18.90	2.38	−0.401	8.865	1.908	52.9	5.247
67344	8.340	31.78	1.06	0.052	6.897	1.443	31.5	4.408
68936	8.356	26.14	1.18	0.444	6.952	1.404	38.3	4.039
69075	9.495	28.79	1.36	−0.490	7.700	1.795	34.7	4.996
69301	10.760	15.21	2.44	−0.208	9.219	1.541	65.7	5.130
69357	7.938	43.35	1.40	−0.081	6.360	1.578	23.0	4.545
69570	8.235	27.62	1.12	−0.557	6.992	1.243	36.2	4.198
71673	10.203	16.33	1.62	−0.182	8.726	1.477	61.2	4.791

Table 17. Continued.

Field stars								
(1) HIP	(2) V (mag)	(3) π (mas)	(4) σ_π (mas)	(5) $[Fe/H]$ (dex)	(6) J (mag)	(7) $V-J$ (mag)	(8) d (pc)	(9) M_J (mag)
72312	7.761	50.84	1.04	−0.123	6.151	1.610	19.7	4.682
72339	8.046	33.60	1.51	0.133	6.712	1.334	29.8	4.344
72577	9.073	32.53	1.56	−0.301	7.313	1.760	30.7	4.874
72688	7.804	58.96	1.05	−0.027	5.990	1.814	17.0	4.843
72703	8.380	25.68	1.29	−0.386	7.118	1.262	38.9	4.166
73547	7.736	36.84	0.98	−0.522	6.419	1.317	27.1	4.251
73963	10.343	13.57	1.91	−0.116	8.770	1.573	73.7	4.433
75266	8.281	39.35	1.37	0.155	6.596	1.685	25.4	4.571
80043	8.901	38.80	1.37	−0.456	7.116	1.785	25.8	5.060
80700	8.807	21.50	1.27	0.314	7.419	1.388	46.5	4.081
81237	8.756	25.32	1.15	−0.149	7.369	1.387	39.5	4.386
84164	9.186	17.74	1.51	−0.304	7.550	1.636	56.4	3.795
85425	7.879	32.04	1.24	−0.432	6.591	1.288	31.2	4.119
87089	8.912	26.16	1.16	−0.112	7.337	1.575	38.2	4.425
88553	8.460	26.99	1.19	−0.149	7.146	1.314	37.1	4.302
89497	8.545	27.11	1.20	−0.088	7.181	1.364	36.9	4.347

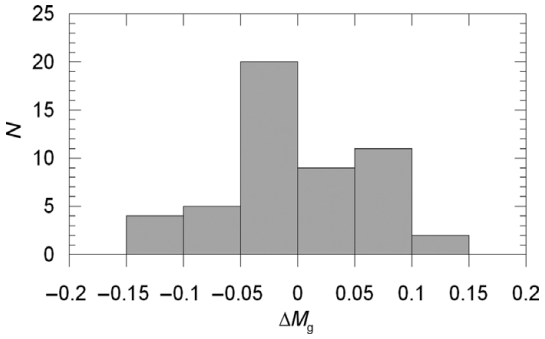

Figure 10. Histogram of the residuals.

used a set of field stars, additional to the Galactic cluster M5 ($[Fe/H] = -1.40$ dex), for the application of the $M_J \times [Fe/H]$ calibration. We tried to apply the procedure to a metal-poor cluster, i.e., M15 whose metallicity is close to the one of M92. But we noticed that the residuals were decreasing systematically from $\Delta M = 0.51$ to $\Delta M = -0.26$ mag in the colour range $0.95 \leq (V-J)_0 \leq 1.40$ mag. Comparison of the absolute magnitude–colour diagrams of the clusters M92 and M15 (Figure 11c) revealed that the reason **for** the systematic variation of the residuals is due to the fiducial sequence of the cluster M15. Actually, although the absolute magnitudes evaluated for M92 and M15 for the colour $(V-J)_0 = 0.95$ mag are close to each other, the absolute magnitudes of M15 deviate from the ones of M92 up to $\Delta M = 0.51$ mag at redder colours. Hence, the systematic residuals in question do not originate from our procedure but they are due to the fiducial sequence of the cluster M15. The fiducial sequences of the clusters M92 and M15 are taken from the same source, i.e. Brasseur et al. (2010). The metallicities for both clusters are given as $[Fe/H] = -2.4$ dex in

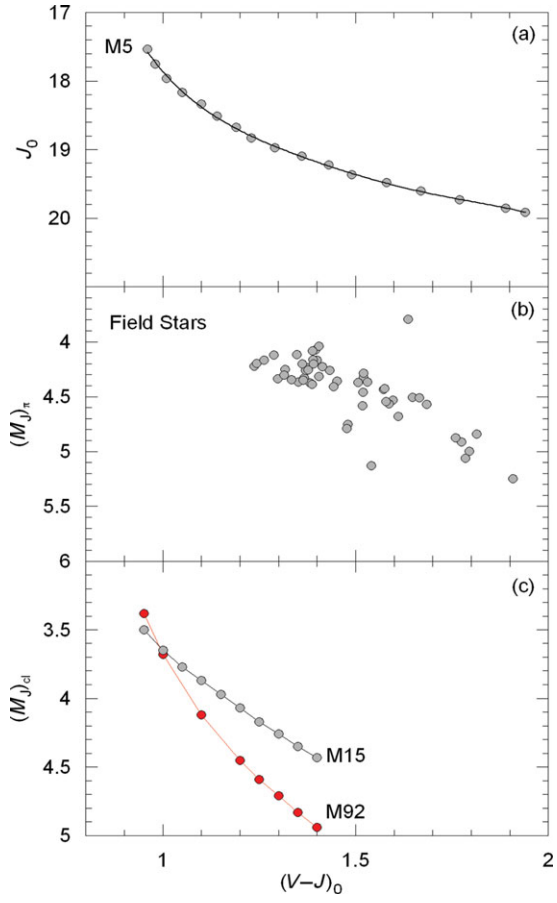

Figure 11. $J_0 \times (V-J)_0$ colour-apparent magnitude diagram of the cluster M5 (panel a), distribution of the field stars with solar metallicity in the $(V-J)_0$ colour versus $(M_J)_\pi$ absolute magnitude diagram (panel b), and deviation of the $(V-J)_0$ colour $(M_J)_{cl}$ absolute magnitude diagram of the cluster M15 (brighter magnitudes) from the one of M92 (fainter magnitudes).

Table 18. Absolute magnitudes $(M_J)_{ev}$ and residuals ΔM estimated by the procedure explained in our work. $(M_J)_{cl}$ and $(M_J)_{\pi}$ denote the absolute magnitudes evaluated by means of the colour-magnitude diagram of the M5 cluster and the parallax of the field star, respectively.

Table 18a

(1) $(V-J)_0$ (mag)	(2) $(M_J)_{cl}$ (mag)	(3) $(M_J)_{ev}$ (mag)	(4) ΔM (mag)	(1) $(V-J)_0$ (mag)	(2) $(M_J)_{cl}$ (mag)	(3) $(M_J)_{ev}$ (mag)	(4) ΔM (mag)		
0.95	3.11	3.20	−0.09	1.37	4.74	4.68	0.06	–	–
0.97	3.27	3.34	−0.08	1.40	4.80	4.73	0.07	–	–
1.00	3.48	3.52	−0.04	1.43	4.86	4.79	0.06	–	–
1.03	3.66	3.67	−0.01	1.45	4.89	4.83	0.06	–	–
1.05	3.77	3.75	0.02	1.47	4.93	4.87	0.06	–	–
1.07	3.87	3.83	0.04	1.50	4.98	4.93	0.05	–	–
1.10	4.00	3.93	0.07	1.53	5.03	4.98	0.05	–	–
1.13	4.12	4.03	0.09	1.55	5.06	5.02	0.04	–	–
1.15	4.19	4.09	0.10	1.57	5.09	5.05	0.04	–	–
1.17	4.25	4.15	0.11	1.60	5.13	5.10	0.03	–	–
1.20	4.34	4.27	0.08	1.63	5.17	5.15	0.02	–	–
1.23	4.43	4.33	0.09	1.65	5.20	5.18	0.02	–	–
1.25	4.48	4.38	0.10	1.67	5.22	5.21	0.01	–	–
1.27	4.53	4.43	0.10	1.70	5.26	5.26	0.00	–	–
1.30	4.59	4.50	0.10	1.73	5.29	5.30	−0.01	–	–
1.33	4.66	4.58	0.08	1.75	5.31	5.32	−0.01	–	–
1.35	4.70	4.63	0.07	–	–	–	–	–	–

Table 18b

(1) $V-J$ (mag)	(2) $(M_J)_{\pi}$ (mag)	(3) $[Fe/H]$ (dex)	(4) $(M_J)_{ev}$ (mag)	(5) ΔM (mag)	(1) $V-J$ (mag)	(2) $(M_J)_{\pi}$ (mag)	(3) $[Fe/H]$ (dex)	(4) $(M_J)_{ev}$ (mag)	(5) ΔM (mag)
1.24	4.22	−0.29	3.87	0.35	1.41	4.31	−0.25	4.32	−0.01
1.24	4.20	−0.56	4.01	0.19	1.41	4.23	0.04	4.19	0.04
1.26	4.17	−0.39	3.98	0.19	1.43	4.26	0.33	4.09	0.17
1.29	4.12	−0.43	4.09	0.03	1.44	4.41	0.05	4.25	0.16
1.30	4.34	−0.24	4.02	0.32	1.45	4.36	−0.16	4.36	0.00
1.31	4.30	−0.15	4.01	0.29	1.48	4.79	−0.18	4.44	0.35
1.32	4.25	−0.52	4.23	0.02	1.48	4.75	−0.32	4.49	0.26
1.33	4.34	0.13	3.95	0.39	1.51	4.37	−0.20	4.51	−0.14
1.35	4.12	0.37	3.88	0.24	1.52	4.58	−0.21	4.53	0.05
1.35	4.37	−0.10	4.12	0.25	1.52	4.46	−0.04	4.46	0.00
1.36	4.20	−0.22	4.20	0.00	1.52	4.33	0.31	4.29	0.04
1.36	4.35	−0.09	4.14	0.21	1.52	4.28	−0.29	4.57	−0.29
1.37	4.33	−0.32	4.28	0.05	1.53	4.36	0.02	4.45	−0.09
1.37	4.26	0.06	4.09	0.17	1.54	5.13	−0.21	4.57	**0.56**
1.38	4.26	0.03	4.13	0.13	1.57	4.43	−0.12	4.60	−0.17
1.38	4.24	−0.48	4.36	−0.12	1.58	4.43	−0.11	4.61	−0.18
1.38	4.38	−0.07	4.18	0.20	1.58	4.54	−0.08	4.60	−0.06
1.39	4.39	−0.15	4.23	0.16	1.59	4.57	−0.09	4.63	−0.06
1.39	4.08	0.31	4.01	0.07	1.60	4.53	0.03	4.59	−0.06
1.39	4.16	0.13	4.10	0.06	1.61	4.68	−0.12	4.68	0.00
1.39	4.20	0.01	4.16	0.04	1.64	3.79	−0.30	4.82	**−1.03**
1.40	4.07	0.03	4.17	−0.10	1.65	4.51	0.09	4.66	−0.15
1.40	4.17	0.21	4.09	0.08	1.67	4.51	0.14	4.67	−0.16
1.40	4.04	0.44	3.97	0.07	1.69	4.57	0.16	4.71	−0.14

the same paper. Additionally, they have the same age, a bit less than 13 Gyr (Salaris, degl'Innocenti, & Weiss 1997). Hence, the problem related to the discrepancy between the two fiducial sequences could not be solved.

We compared the absolute magnitudes estimated by the procedure explained in our paper with those evaluated either by combination of the J_0, $(V-J)_0$ fiducial sequence of the cluster M5 and its true distance modulus or by the J_0 apparent magnitude and the distance of the field star in question. The total residuals lie between -0.29 and $+0.39$ mag. However, the range of 87% of them is rather shorter, i.e. $-0.20 < \Delta M \leq +0.20$ mag. The mean and the standard deviation of all residuals are $< \Delta M >= 0.05$ and $\sigma = 0.13$ mag. However, we state that the cluster fiducials

Table 19. Distribution of the residuals. N denotes the number of stars.

ΔM_J-interval (mag)	$< \Delta M_J >$ (mag)	N
(−0.3, −0.2]	− 0.29	1
(−0.2, −0.1]	− 0.15	8
(−0.1, 0.0]	− 0.03	16
(0.0, 0.1]	0.06	36
(0.1, 0.2]	0.16	9
(0.2, 0.3]	0.25	5
(0.3, 0.4]	0.35	4

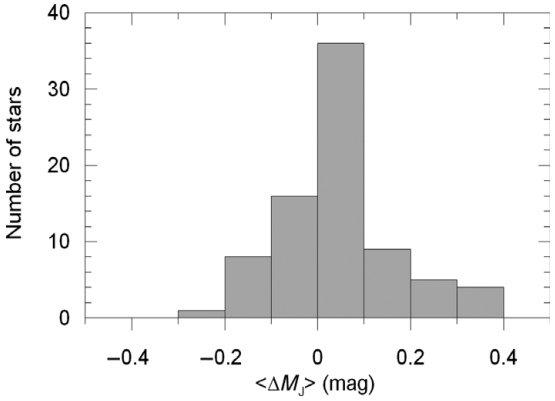

Figure 12. Histogram of the residuals.

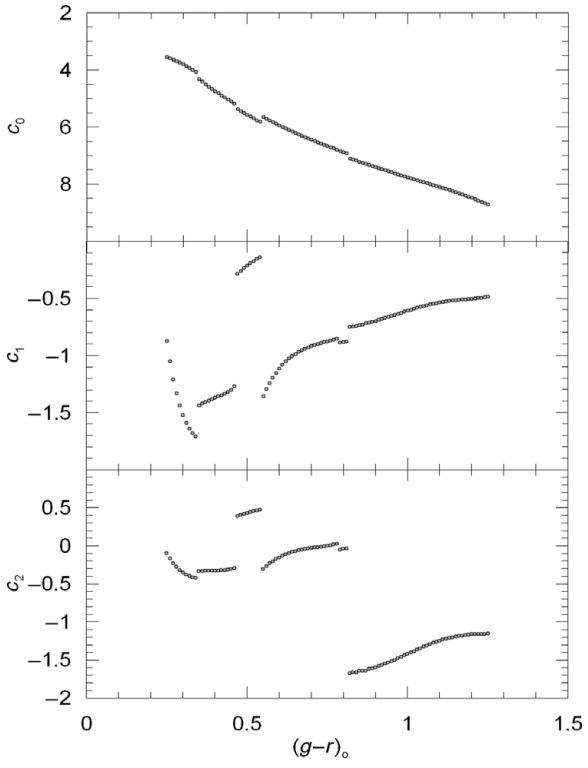

Figure 13. Variation of c_0, c_1, and c_2 coefficients with colour index $(g-r)_0$ in three panels.

Table 20. Data for two young clusters.

Cluster	$E(B-V)$ (mag)	μ_0 (mag)	$[Fe/H]$ (dex)	t (Gyr)	Ref
NGC 3680	0.058	9.89	−0.08	1.75	1, 2
NGC 2158	0.440	12.80	−0.25	2.00	3, 4

(1) Cummings et al. (2012), (2) Eggen (1969), (3) Smolinski et al. (2011), (4) Saad & Lee (2001).

provide more accurate absolute magnitudes than the ones for the field stars. Thus, the absolute magnitude M_J of a dwarf would be determined with an accuracy of $\Delta M < 0.2$ mag. The mean and standard deviation of the residuals estimated with the same photometry (V, J) for red giants were $< \Delta M >= 0.137$ and $\sigma = 0.080$ mag (Karaali et al. 2013b) which indicates that the absolute magnitudes of dwarfs would be determined with better accuracy. The reason of this improvement is the same as stated for the absolute magnitude M_g. The calibration of M_g and M_J in terms of $[Fe/H]$ is carried out in steps of 0.01 mag. A small step is necessary to isolate an observational error on $g-r$ and $V-J$ plus an error due to reddening. The origin of the mentioned errors shows the trend of the dwarf sequence. However, we note that the dwarf sequence is not steep. Hence, contrary to the red giant branch sequence Karaali et al. (2013a), an error in $(g-r)$ or $(V-J)$ does not imply a large change in the absolute magnitude.

The c_i and d_i $(i = 0, 1, 2)$ coefficients in Tables 9 and 12, respectively, are colour-dependent. Additionally, it seems that there is a smooth relation between a given c_i or d_i coefficient and the $(g-r)$ and $(V-J)$ colour. We confirmed this argument by plotting each c_i coefficient versus $(g-r)_0$ colour. Actually, each panel in Figure 13 consists of a set of smooth relations with breaks at $(g-r)_0$ colours where the number of clusters employed in the $[Fe/H]$ calibrations changes. It is interesting, the mentioned breaks in the panel c_0 versus $(g-r)_0$ are so small that one can assume a continuous relation for the whole colour interval, i.e. $0.25 \leq (g-r)_0 \leq 1.25$ mag. The mentioned relation originates from the fact that $M_g = c_0$ for $[Fe/H] = 0$ dex.

The procedure for absolute magnitude calibration for dwarfs in Karaali et al. (2003) is based on the absolute magnitude offset which is defined as a function of ultraviolet excess. However, ultraviolet excess can not be provided easily with SDSS, especially for late-type stars, and this parameter has not been defined in 2MASS system. Whereas, the procedure in this study is metallicity-dependent, and metallicity values come from detailed analysis of individual stars using high-resolution spectroscopy in large surveys which are in operation, such as RAVE, SEGUE, *GAIA*-ESO, and APOGEE or which will be started in the near future, such as GALAH.

SDSS and 2MASS are two of the widely used photometric systems in the Galactic researches. Also, our procedure covers dwarfs with a large metallicity and age range. The metallicity range is $-2.15 \leq [Fe/H] \leq 0.37$ dex in both systems, while the age ranges are defined by the clusters used for the calibrations in SDSS and 2MASS, i.e. $4 \leq t \leq 13.2$ and $2 \leq t \leq 13.2$ Gyr, respectively, where 2, 4 and 13.2 Gyr are the ages of the clusters NGC 2158, M67 and M92. The age of the cluster NGC 2158 is taken from Carraro, Girardi, & Marigo (2002), while those for the clusters M67 and M92 were estimated in Karaali et al. (2012). Additionally, the mean residuals and standard deviations in the application of two absolute magnitude calibrations, M_g and M_J, are small. Hence, the procedure presented in this paper can be applied with a good accuracy to large samples of dwarf stars in Galactic-structure Projects.

We stated in our previous papers (Karaali et al. 2012) that our absolute magnitude calibrations are age-restricted, i.e., they cover the stars with ages in the range defined by the youngest and oldest clusters used in the calibration. We applied the calibration $M_g \times [Fe/H]$ to two clusters, NGC 3680 and NGC 2158, younger than 4 Gyr to test the age range in the SDSS system. We used the V and $B-V$ data of the cluster NGC 3680 in Kozhurina-Platais et al. (1997) and reduced them to the g_0 magnitude and $(g-r)_0$ colour by means of the equations of Chonis & Gaskell (2008) given in Section 3.2.1, after necessary corrections for interstellar extinction. The colours and magnitudes of the cluster NGC 2158 taken from Smolinski et al. (2011) are already in the SDSS system. The $M_g \times [Fe/H]$ calibration could be applied to nine stars in NGC 3680 and 10 fiducials in NGC 2158, and the absolute magnitude residuals for each set of data were estimated. The mean residuals are very similar and rather high, i.e. $< \Delta M >= 1.25$ mag for 9 stars and $< \Delta M >= 1.20$ mag. for 10 fiducials, which shows that the calibration in question is limited with the age of the youngest cluster used for the calibration, i.e., 4 Gyr. The metallicities of the clusters NGC 3680 and NGC 2158 are close to the one of M67 whose age is 4 Gyr, while the ages of the first two clusters are different than the one of M67. A similar test can be carried out for the $M_J \times [Fe/H]$ calibration. Hence, we can argue that our absolute magnitude calibrations are better defined in terms of ranges in age. The colour excesses, distance moduli, metallicities, and ages of the clusters are presented in Table 20. However, the magnitudes and colours used in the evaluation of absolute magnitude residuals are not given in the paper because of space constraints.

ACKNOWLEDGMENTS

The authors would like to thank the anonymous referee who provided valuable comments and for improving the manuscript. This research has made use of NASA(National Aeronautics and Space Administration)'s Astrophysics Data System and the SIMBAD Astronomical Database, operated at CDS, Strasbourg, France.

REFERENCES

Alcaino, G., Liller, W., Alvarado, F., & Wenderoth, E. 1990, ApJS, 72, 693
An, D., et al. 2008, ApJS, 179, 326
Arp, H., & Cuffey, J. 1962, ApJ, 136, 51
Bilir, S., Ak, S., Karaali, S., Cabrera-Lavers, A., Chonis, T. S., & Gaskell, C. M. 2008, MNRAS, 384, 1178
Brasseur, C. M., Stetson, P. B., VandenBerg, D. A., Casagrande, L., Bono, G., & Dall'Ora, M. 2010, AJ, 140, 1672
Breddels, M. A., et al. 2010, A&A, 511, 90
Cardelli, J. A., Clayton, G. C., & Mathis, J. S. 1989, ApJ, 345, 245
Carraro, G., Girardi, L., & Marigo, P. 2002, MNRAS, 332, 705
Chen, B., et al. 2001, ApJ, 553, 184
Chonis, T. S., & Gaskell, C. M. 2008, AJ, 135, 264
Cummings, J. D., Deliyannis, C. P., Anthony-Twarog, B., Twarog, B., & Maderak, R. M. 2012, AJ, 144, 137
Di Criscienzo, M., Marconi, M., & Caputo, F. 2004, ApJ, 612, 1092
Eggen, O. J. 1969, ApJ, 155, 439
ESA 1997, The Hipparcos and Tycho Catalogues, CDS/ADC Electronic Catalogues, 1239
Fan, X. 1999, AJ, 117, 2528
Ferro, A. A., et al. 2011, MNRAS, 416, 2265
Gratton, R. G., Fusi Pecci, F., Carretta, E., Clementini, G., Corsi, C. E., & Lattanzi, M. 1997, ApJ, 491, 749
Harris, W. E. 1996, AJ, 112, 1487
Karaali, S., Bilir, S., & Gökçe, E. Y. 2012, PASA, 29, 509
Karaali, S., Bilir, S., & Gökçe, E. Y. 2013a, PASA, 30, 8
Karaali, S., Bilir, S., & Gökçe, E. Y. 2013b, PASA, 30, 11
Karaali, S., Bilir, S., & Tunçel, S. 2005, PASA, 22, 24
Karaali, S., Karataş, Y., Bilir, S., Ak, S. G., & Hamzaoğlu, E. 2003, PASA, 20, 270
Kozhurina-Platais, V., Demarque, P., Platais, I., Orosz, J. A., & Barnes, S. 1997, AJ, 113, 1045
Laird, J. B., Carney, B. W., & Latham, D. W. 1988, AJ, 95, 1843
McCall, M. L. 2004, AJ, 128, 2144
Nissen, P. E., & Schuster, W. J. 1991, A&A, 251, 457
Phleps, S., Meisenheimer, K., Fuchs, B., & Wolf, C. 2000, A&A, 356, 108
Reid, I. N. 1997, AJ, 114, 161
Saad, S. M., & Lee, S. 2001, JKAS, 34, 99
Salaris, M., degl'Innocenti, S., & Weiss, A. 1997, ApJ, 479, 665
Sarajedini, A., Brandt, K., Grocholski, A. J., & Tiede, G. P. 2004, AJ, 127, 991

Sarajedini, A., Mathieu, R. D., & Platais, I. 2003, ASSL, 289, 257
Siegel, M. H., Majewski, S. R., Reid, I. N., & Thompson, I. B. 2002, ApJ, 578, 151
Skrutskie, M. F., et al. 2006, AJ, 131, 1163
Smolinski, J. P., et al. 2011, AJ, 141, 89
von Hippel, T., Steinhauer, A., Sarajedini, A., & Deliyannis, C. P. 2002, AJ, 124, 1555
York, D. G., et al. 2000, AJ, 120, 1579
Zwitter, T., et al. 2010, A&A, 522, 54